



City Research Online

City, University of London Institutional Repository

Citation: Patsialis, D., Taflanidis, A. & Giaralis, A. (2023). Exploring the impact of excitation and structural response/performance modeling fidelity in the design of seismic protective devices. *Engineering Structures*, 291, 115811. doi: 10.1016/j.engstruct.2023.115811

This is the accepted version of the paper.

This version of the publication may differ from the final published version.

Permanent repository link: <https://openaccess.city.ac.uk/id/eprint/29825/>

Link to published version: <https://doi.org/10.1016/j.engstruct.2023.115811>

Copyright: City Research Online aims to make research outputs of City, University of London available to a wider audience. Copyright and Moral Rights remain with the author(s) and/or copyright holders. URLs from City Research Online may be freely distributed and linked to.

Reuse: Copies of full items can be used for personal research or study, educational, or not-for-profit purposes without prior permission or charge. Provided that the authors, title and full bibliographic details are credited, a hyperlink and/or URL is given for the original metadata page and the content is not changed in any way.

City Research Online:

<http://openaccess.city.ac.uk/>

publications@city.ac.uk

Exploring the impact of excitation and structural response/performance modeling fidelity in the design of seismic protective devices

D. Patsialis^a, A.A Taflanidis^a and A. Giaralis^b

^a*Department of Civil & Environmental Engineering & Earth Sciences, University of Notre*

Dame, Notre Dame, IN 46556, USA

^b*Department of Engineering, City, University of London, EC1V 0HB, London, UK*

Abstract

The design of seismic protective devices (SPDs), such as fluid viscous dampers (VDs), and inertial vibration absorbers (IVAs), requires the adoption of appropriate models for: (i) the earthquake excitation description (e.g. stochastic stationary/non-stationary versus recorded ground motions); (ii) the seismic structural response estimation (e.g. linear versus nonlinear/hysteretic); and (iii) the seismic performance quantification (e.g. average response versus risk-based performance description). This paper pursues a novel detailed investigation of the impact of modeling fidelity in the design of SPDs, by examining different combinations of models with different levels of sophistication for each of the aforementioned aspects. In this manner, a large model hierarchy is established, resulting in multiple SPD design variants. A bi-objective optimal design formulation is adopted, considering the competing structural vibration suppression (building performance) and device control forces as distinct performance objectives (POs). Comprehensive comparisons are reported for a 3-storey and a 9-storey steel benchmark building, equipped with distributed VDs in all floors and with different types of single-device IVAs including the tuned-inerter-damper (TID), the tuned-mass-damper-inerter (TMDIs) and the tuned-mass-damper (TMD). An innovative methodological approach is established to gauge the impact of the model fidelity by examining the deviation of POs achieved by lower fidelity SPD designs versus the Pareto-optimal fronts corresponding to POs consistent with the higher fidelity assumptions. It is found that the TID is more robust than the TMDI to design modelling assumptions, suggesting that more lightweight IVAs (where

majority of secondary mass is replaced by inertance property) relax requirements for high-fidelity models in device tuning. It is further found that large force VD's installed in each building floor are significantly more robust to the design fidelity modelling than single IVA implementations at the expense of increased costs to accommodate the larger number of devices. Consideration of structural nonlinear response becomes important in the SPD design when combined with risk-based performance quantification as opposed to average performance (i.e. the popular \mathcal{H}_2 design). Moreover, the risk-based performance of nonlinear structures becomes sensitive to the use of recorded ground motions (GMs) as opposed to artificial GMs with only time-domain non-stationarity, as well as to the number of recorded GMs used. The study overall stresses that the use of lower fidelity models may provide sub-optimal performance in certain settings, and that comparison across the model hierarchy can be leveraged to obtain key insights of the SPD behavior. Additional key findings pertain to the robustness characteristics of the different type of SPDs to the modeling assumptions utilized for the device design.

Keywords: seismic protective device design; model fidelity; risk-based design; non-stationary performance; reduced order modeling.

1. Introduction

The design of seismic protective devices (SPDs), such as fluid viscous dampers (VDs) [1-3], tuned mass dampers (TMDs) [4-8] or inerter-based vibration absorbers (IVAs) [9-11], requires appropriate descriptions for the excitation, the structural response, and the seismic performance. The combination of these descriptions ultimately reflects the objective function definition of the SPD design optimization problem. A wide range of descriptions, with different levels of sophistication, have been considered in the literature to address the optimal SPD design. Common simplified approaches adopt the transfer function amplification for the fundamental (or first few) structural vibration mode(s) [12-16] as the objective function to be minimized. Alternative simplified approaches seek to achieve a specific target value for the damping ratio (or energy dissipation), frequently obtained through some approximation for the device

Patsialis D, Taflanidis AA, Giaralis A (2023) Exploring the impact of excitation and structural response/performance modeling fidelity in the design of seismic protective devices. *Engineering Structures*, Accepted 13/2/2023.

characteristics or structural response [17, 18]. In other studies, the seismic excitation is modelled as stationary Gaussian random process with site-specific spectral properties, while assessment is pursued by the second-order statistics of the stochastic response obtained through random vibrations analysis [9, 19-21]. Alternatively, first-passage reliability-criteria for more elaborate seismic performance quantification have been adopted in conjunction with stationary seismic excitation description [22-24]. More advanced methodologies adopt a non-stationary seismic excitation description and make use of time-history analysis and peak response quantities to evaluate seismic performance [25-27]. In the latter methodologies, the characterization of seismic performance ranges from the aggregation of results over a small ensemble of ground motions [21, 28, 29] [30, 31] to the comprehensive risk analysis through probabilistic frameworks [32] that might even include life-cycle performance considerations [33-35]. Though the majority of studies assume linear structural response, some approaches account for the potential hysteretic behavior of structures [7, 36-38].

In this setting, the fidelity of the models adopted for describing the excitation, estimating structural response and quantifying performance may drastically impact the design of SPDs. Higher fidelity models, such are those adopting nonlinear response history analysis (NLRHA) and performance-based earthquake engineering (PBEE) principles [38, 39], may potentially achieve a more realistic representation of the actual (expected) performance, but entail a very large computational burden for performing the device design optimization. This large burden is frequently mitigated by considering some type of approximation in the optimization problem definition and solution. Examples include the use of global surrogate modelling techniques to replace the original performance objective with an inexpensive approximation [34] or the formulation of the problem so that the number of design variables is kept moderately small. On the other hand, simpler models can accommodate a solution of the optimal SPD design problem at a small fraction of the computational cost compared to high-fidelity models but are expectedly less accurate in the design problem description. Still, these models might identify optimal SPD designs that are consistent with approaches that use higher-fidelity models, achieving ultimately similar performance.

To this end, the following question related to model parsimony becomes critical in the design of SPDs: what should be the level of sophistication of the seismic excitation, structural response and performance quantification models to identify useful SPD designs for seismic protection of building structures? This study addresses this question by investigating in detail the impact of modeling fidelity on the design of SPDs. To achieve this objective, all the different aspects of the SPD design problem formulation are considered: characterization of dynamic/earthquake excitation, estimation of structural response, and quantification of performance. In this junction, it is noted that a number of studies have tried to address similar questions in the past [38, 40, 41][42]. Though these studies have made critical contributions to the field of optimal seismic SPD design, they also share some limitations. Firstly, they examined limited number of SPD types. Further, they considered a single design objective, inadvertently restricting emphasis on a specific range for the SPD vibration mitigation efficiency. Moreover, they focused on only one of the three aspects/descriptors of the SPD design problem formulation, or adopted fundamentally different descriptions, failing to investigate in detail foundational differences of specific aspects of this formulation. For example, the study in [42] made a comparison between different performance quantifications for only stationary random excitation. Further, the work in [40] and [41] compared mean squared stationary designs to designs that use detailed seismic-risk descriptions and life-cycle performance quantifications, respectively. In contrast, the present study establishes hierarchical models across the three aspects/descriptors of the design problem formulation. This novel consideration allows for consistent comparisons among the different levels of model fidelity, looking at both the individual descriptor as well as at the hierarchy of models. In this respect, ultimately, multiple variants of the design problem with increasing degree of complexity are examined for the first time in the literature. Three different SPDs are studied: VDs and two IVAs, specifically the tuned-mass-damper-inerter (TMDI) [43] and the tuned-inerter-damper (TID) [9, 11], with the TMD being a special case of the TMDI (without an inerter). Additionally, a bi-objective design is adopted, considering both the structural vibration suppression and the device control forces as separate performance objectives. This consideration enables comparisons across a wide range of

Patsialis D, Taflanidis AA, Giaralis A (2023) Exploring the impact of excitation and structural response/performance modeling fidelity in the design of seismic protective devices. *Engineering Structures*, Accepted 13/2/2023.

the SPD vibration efficiency. For structural performance, designs that consider suppression of inter-story drifts, absolute floor accelerations, or combination of both are separately considered to facilitate more comprehensive comparisons. All these features constitute the novel contributions of the present study.

Specifically, for the excitation, both stationary and non-stationary descriptions are examined. For the non-stationary implementation, the use of either a stochastic ground motion model, established through an extension of the stationary description using a time-domain envelope function, or of an ensemble of recorded ground motion are considered. Consistency across the different excitation modeling approaches is achieved by establishing compatibility of the corresponding response spectrum. For the structural response, the use of either linear or nonlinear, hysteretic structural models are examined. A higher-fidelity, finite element model (FEM) is assumed, developed in OpesSees [44] in the illustrative case studies. Static condensation of that FEM provides the linear structural model. Further, to facilitate the design optimization when examining nonlinear structural response, the reduced order modeling framework recently developed by the first two authors is adopted [45], to derive a computational efficient low-order nonlinear model from a detailed nonlinear OpenSees FEM. For the structural performance quantification, both average responses and a risk-based description following current PBEE standards are examined. The risk-based quantification is established by considering the consequences associated with engineering demand parameters (EDPs), such as inter-story drifts and absolute floor accelerations, exceeding threshold values representative of different damage states. When utilizing stationary excitation description, average performance is quantified through the root mean-squared responses (\mathcal{H}_2 design), while the risk-based performance is quantified utilizing first-passage random vibration theory. When utilizing non-stationary excitation description, average performance is quantified through the median peak responses, while the risk-based performance is quantified through vulnerability functions based on the peak EDPs. It should be stressed that several other modeling assumptions could have been made, and the ones considered here by no means correspond to an exhaustive list. However, they represent common choices utilized in the design of SPDs, and facilitate a hierarchical description of models across the three critical aspects of the problem formulation. One

Patsialis D, Taflanidis AA, Giaralis A (2023) Exploring the impact of excitation and structural response/performance modeling fidelity in the design of seismic protective devices. *Engineering Structures*, Accepted 13/2/2023.

additional aspect of this formulation that is not investigated in this study is the modeling fidelity of the SPD itself. A number of studies have examined the impact of nonlinearities in the SPD description [46-53]. To properly examine this impact, all other aspects of the problem formulation should be kept the same, to isolate the influence of the device-specific modeling assumptions on the design driven by the particular SPD technology. For these reasons, this fidelity comparison falls outside the scope of this study.

The remaining of the paper is organized as follows. Sections 2, 3 and 4 present, respectively, the models for the excitation, structural response and performance quantification. Section 5 discusses the design problem formulation and its numerical solution. Details for the illustrative case study are presented in Section 6, followed by the discussion of the results and the detailed evaluation of the impact of the model fidelity in Section 7. Section 8 summarizes the key trends identified in Section 7 and offers the conclusions of this study.

2. Seismic excitation description

For the seismic excitation description, represented by the ground acceleration $\ddot{x}_g(t)$, where t corresponds to time, both stationary and non-stationary modeling is examined, with two alternative approaches used for the non-stationary formulation. The stationary description, denoted by S hereafter, represents a lower fidelity approximation, modeling the acceleration time-history of the ground motion as a stationary stochastic process. This stationary stochastic model may be reasonable for approximating the steady-state component of the structural response under the strong part of the seismic excitation [54]. The non-stationary description offers a refined representation of acceleration time-histories by either using non-stationary stochastic models [55-57], hereafter indicated as NS description, or utilizing past, recorded ground motions [58], hereafter indicated as NS_r description. Consistency across the alternative seismic excitation descriptions is achieved by ensuring that the median response spectra of the descriptions match well the same (given) design response spectrum.

At this point it is important to remind the reader that that a non-stationary representation of the seismic action is always more realistic than a stationary one. However, as discussed in the introduction, stationary seismic excitation assumption has been (and is still) widely considered when it comes to optimal design/tuning of various SPDs, with non-stationary seismic excitation used in many studies only to assess numerically the effectiveness of the SPDs (designed/tuned using a stationary assumption for the excitation). The consideration of stationary excitation, therefore, supports the objective of this study, which is to assess what difference it makes when assuming stationary as opposed to different types of non-stationary seismic representations in the design/tuning of the SPDs.

2.1 Stationary description

For the stationary seismic excitation description, the ground acceleration, $\ddot{x}_g(t)$ is approximated as a stationary Gaussian stochastic process with power spectral density $S_g(\omega)$, where ω denotes frequency. In the illustrative example considered later, a high-pass filtered Kanai-Tajimi power spectrum is adopted [54]:

$$S_g(\omega) = s_o \frac{\omega_g^4 + 4\zeta_g^2 \omega^2 \omega_g^2}{(\omega_g^2 - \omega^2)^2 + 4\zeta_g^2 \omega_g^2 \omega^2} \frac{\omega^4}{(\omega_f^2 - \omega^2)^2 + 4\zeta_f^2 \omega_f^2 \omega^2}. \quad (1)$$

In the above expression, ω_g , ζ_g , ω_f , ζ_f and s_o corresponding to the Kanai-Tajimi parameters, the first four representing the frequency/damping pair of the nominal and high-pass components of the filter, respectively, and the last one controlling the filter amplitude, and chosen based on the desired root mean square ground acceleration a_{RMS} . These parameters are chosen in the illustrative case study in order to establish a match of the underlying median response spectrum of the process to the design response spectrum of the benchmark structures, as detailed in section 6.2. To estimate the stationary response statistics of the structure, required to assess structural performance and to accommodate the extension to the non-stationary excitation description, a state-space formulation may be utilized. This formulation is reviewed in Appendix A.

2.2 Non-stationary description

For the non-stationary seismic excitation description, two popular alternative approaches are considered [59]. The first approach uses a non-stationary stochastic ground motion model to obtain sample realizations of $\ddot{x}_g(t)$. Though a number of such models exist [56], the implementation chosen here is based on uniformly modulating in time the stationary excitation with power spectral density $S_g(\omega)$ in Eq. (1) through an analytically defined temporal envelop function $e_t(t)$ [55, 57]. This choice results in a non-stationary excitation with the same frequency characteristics as the stationary description in Eq. (1). Utilizing the state-space representation of Appendix A, the non-stationary time-history excitation is obtained by modifying the output equation of Eq. (A.1) to be

$$\ddot{x}_g(t) = e_t(t) \mathbf{C}_q \mathbf{x}_q(t) \quad (2)$$

For the envelope function the commonly-used function proposed by Housner and Jennings [60] is adopted in the illustrative case study examined later, given by

$$e_t(t) = \begin{cases} (t/T_r)^2 & \text{for } t < T_r \\ 1 & \text{for } T_r \leq t \leq T_r + T_p \\ e^{-\alpha(t-T_r-T_p)} & \text{for } t > T_r + T_p. \end{cases} \quad (3)$$

and consisting of three parts: a quadratic rise of duration T_r , a plateau of duration T_p representing the fully amplitude developed segment, and an exponential decay with rate α . The h th sample realization, denoted as $\ddot{x}_g^h(t)$ of the ground motion, is obtained by using independent identically distributed sequence of Gaussian random variables $\{w^h(kdt) \sim N(0, (1/dt)^2); k=1, \dots, T_t/dt\}$ as input to the state-space representation of $\ddot{x}_g(t)$, where dt is the chosen time-discretization for the excitation description, T_t is the total duration of excitation, and terminology “ $\sim N(a,b)$ ” denotes Gaussian random variable sample with mean a and variance b .

The second approach for the non-stationary excitation description uses recorded ground motions, scaled such that their average response spectrum matches the design spectrum for the examined structural application. Different methodologies exist to accomplish the ground motion selection and scaling [61-63], and the one adopted here is to select ground motions within some desired constraints for secondary features such as significant duration, and then establish a match to the design spectrum for the examined structure by applying an amplitude scaling factor [64] that minimizes the mean-squared error (MSE) between the response and design spectrum, within some period range of interest. This period of interest is selected to be in the range of $0.2T_1$ and $2T_1$, per modern PBEE standards [65], where T_1 is the fundamental period of the structure of interest. Each of these earthquakes represents a different sample $\ddot{x}_g^h(t)$ for the dynamic excitation.

3. Structural model description

For the structural model, both linear (denoted as L) and nonlinear (denoted as NL) models are considered. For achieving computational efficiency in the design of SPDs when considering nonlinear structural response, the framework recently developed by the authors [38] is adopted, leveraging a reduced order model (ROM) formulation [45, 66] to accommodate the adoption of high-fidelity, finite element models (FEMs) within this design.

As discussed in the introduction, two SPD implementations are examined, as also shown in Fig. 1. The first implementation corresponds to fluid viscous dampers (VDs), whose proven efficacy and modeling simplicity make them an attractive seismic protection device for new and existing buildings [2, 3]. The second implementation corresponds to different types of inerter-based vibration absorbers (IVAs), which have recently emerged as promising devices for the earthquake protection of building structures [9, 25, 67, 68], established by coupling viscous and tuned-mass dampers with an inerter [69]. The specific IVAs examined here are the tuned-mass-damper-inerter (TMDI) [9, 43] and the tuned-inerter-damper (TID) [11]. Tuned Mass Dampers (TMDs) are a special case of TMDI (for zero inertance element), therefore this

second SPD implementation also covers TMDs. Hereinafter the term IVA will be used to encompass TID, TMDI and TMD devices.

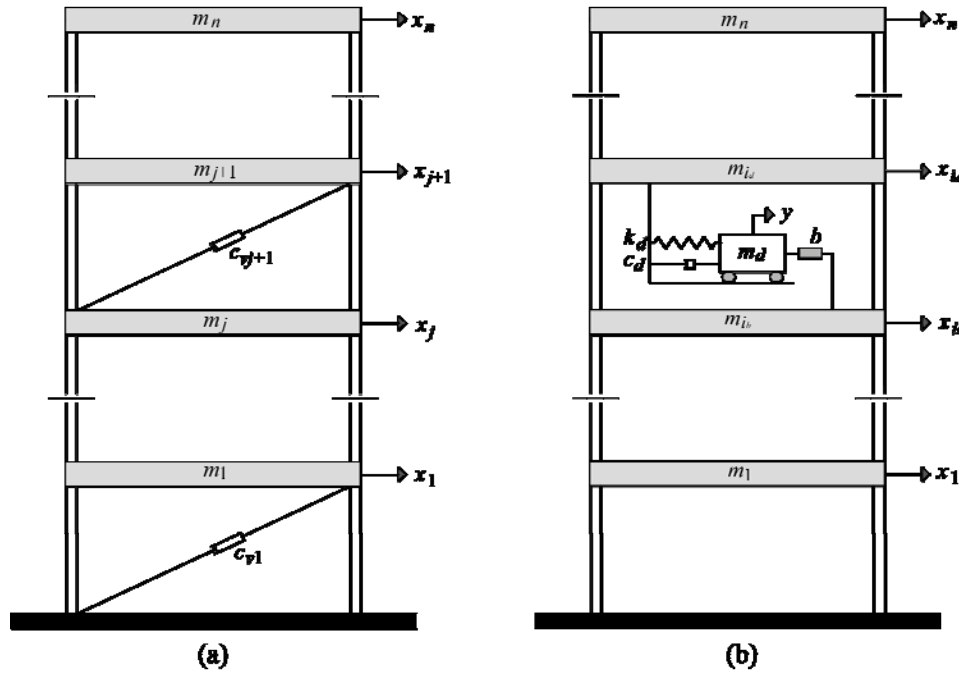


Fig. 1: Structural model equipped with (a) viscous dampers or (b) an inertia device (TMD, TMDI or TID)

The ROM formulation based on a high-fidelity FEM of the structure without the SPD is reviewed in Section 3.1, while Section 3.2 presents the equations of motion for the specific SPDs that will be considered in the illustrative example.

3.1 Reduced order model for structure without the seismic protective device

The formulation of the ROM for a planar structural model (like the one shown in Fig. 1) follows a three-step procedure [45]. In the first step, static condensation is performed for the original FEM, producing the $n \times n$ mass \mathbf{M}_s , linear stiffness \mathbf{K}_s and damping \mathbf{C}_s matrices for the dynamic degrees of freedom (DoF), the latter corresponding to the displacement of each storey relative to the base. The equation of motion for the linear ROM, which matches exactly the dynamic response of the linear FEM, is:

$$\mathbf{M}_s \ddot{\mathbf{x}}_s(t) + \mathbf{C}_s \dot{\mathbf{x}}_s(t) + \mathbf{K}_s \mathbf{x}_s(t) = -\mathbf{M}_s \mathbf{R}_s \ddot{\mathbf{x}}_g(t) \quad (4)$$

Patsialis D, Taflanidis AA, Giaralis A (2023) Exploring the impact of excitation and structural response/performance modeling fidelity in the design of seismic protective devices. *Engineering Structures*, Accepted 13/2/2023.

where $\mathbf{x}_s(t) \in \mathbb{R}^n$ denotes the vector of floor displacements, $\ddot{x}_g(t) \in \mathbb{R}$ represents the ground acceleration and $\mathbf{R}_s \in \mathbb{R}^n$ is the vector of earthquake influence coefficients. In the second step, the linear restoring forces $\mathbf{K}_s \mathbf{x}_s(t)$ in Eq. (4) are replaced with hysteretic ones. Alternative approaches are presented in [45] for accommodating this step, and the one chosen here is to use different hysteretic relationships between each possible combination of DoFs, leading to nonlinear ROM equations of motion:

$$\mathbf{M}_s \ddot{\mathbf{x}}_s(t) + \mathbf{C}_s \dot{\mathbf{x}}_s(t) + \mathbf{T}_c^T \mathbf{f}^c(\mathbf{T}_c \mathbf{x}_s(\tau); \tau \in [0, t] | \mathbf{K}_s, \mathbf{q}) = -\mathbf{M}_s \mathbf{R}_s \ddot{x}_g(t) \quad (5)$$

where \mathbf{T}_c is the $n(n+1)/2 \times n$ connectivity matrix transforming \mathbf{x}_s to the relative displacements across each pair of DoFs, and $\mathbf{f}^c(\mathbf{T}_c \mathbf{x}_s(\tau); \tau \in [0, t] | \mathbf{K}_s, \mathbf{q}) \in \mathbb{R}^{n(n+1)/2}$ is the vector of hysteretic forces between these DoFs. The latter forces, as also indicated by their notational description: (a) are functions of the relative displacement between the DoFs, $\mathbf{T}_c \mathbf{x}_s(\tau)$, for the entire time-history up to time t , $\tau \in [0, t]$; (b) follow some specific hysteretic relationship \mathbf{f}^c that is parameterized through vector \mathbf{q} and corresponds to initial stiffness that matches \mathbf{K}_s . The third step of the formulation is the selection (calibration) of \mathbf{q} , established through a formal optimization with objective the minimization of the discrepancy between the nonlinear FEM and ROM time-history responses for a number of carefully chosen excitations. Details for the hysteretic relationships \mathbf{f}^c that can be considered in this context, as well as for efficiently performing the optimization associated with their calibration (selection of \mathbf{q}), including the selection of excitations, can be found in [45]. Extension of the calibration within a Bayesian setting is discussed in [70].

3.2 Reduced order model for structure with the seismic protective device

Since the addition of SPD does not alter the hysteretic behavior characteristics of the FEM, the ROM calibration does not need to be re-examined once the SPD is added. Simply the equations of motion need to be adjusted. The validation of this concept has been already demonstrated in [38].

For a structure with l VD's shown in Fig. 1(a), let $\mathbf{R}_v = [\mathbf{r}_{v1}, \dots, \mathbf{r}_{vl}]$ be the damping influence coefficient matrix, with the i^{th} row corresponding to the influence row vector $\mathbf{r}_{vi} \in \mathbb{R}^n$ of the i^{th} damper. If the i^{th} damper

is placed between j and $j+1$ floor, then the $j+1$ element of \mathbf{r}_{vi} is 1, the j element is -1 and all other elements are zero. Considering ideal VDs, the equation of motion of the ROM is:

$$\mathbf{M}_s \ddot{\mathbf{x}}_s(t) + \mathbf{C}_s \dot{\mathbf{x}}_s(t) + \mathbf{R}_v^T \text{diag}(\mathbf{c}_v) \mathbf{R}_v \dot{\mathbf{x}}_s(t) + \mathbf{T}_c^T \mathbf{f}^c(\mathbf{T}_c \mathbf{x}_s(\tau); \tau \in [0, t] | \mathbf{K}_s, \mathbf{q}) = -\mathbf{M}_s \mathbf{R}_s \ddot{\mathbf{x}}_g(t) \quad (6)$$

where $\text{diag}(\mathbf{c}_v)$ corresponds to a diagonal matrix with elements the damping coefficients of each damper, with the damping coefficient for the i th damper denoted as c_i . For the i th damper, its force, denoted as f_i , which will be also needed in the design problem formulation, is given by:

$$f_i = c_i \mathbf{r}_{vi} \dot{\mathbf{x}}_s(t) \quad (7)$$

For IVAs, the equations of motion formulation of study [26] is adopted. TMDI is modeled as a secondary mass m_d connected to the i_d DoF through a spring k_d and dashpot c_d , and to the i_b DoF through an inerter with inertance b . The TID and TMD are modeled as special cases with $m_d=0$ and $b=0$, respectively. If $y(t) \in \mathbb{R}$ is the displacement of the mass m_d relative to the i_d floor, the equations of motion of the structure with the inertia-based SPD are:

$$\begin{aligned} (\mathbf{M}_s + \mathbf{R}_d m_d \mathbf{R}_d^T + \mathbf{R}_c b \mathbf{R}_c^T) \ddot{\mathbf{x}}_s(t) + (\mathbf{R}_d m_d + \mathbf{R}_c b) \dot{y}(t) + \mathbf{C}_s \dot{\mathbf{x}}_s(t) + \mathbf{f}^c(\mathbf{T}_c \mathbf{x}_s(\tau); \tau \in [0, t] | \mathbf{K}_s, \mathbf{q}) \\ = -(\mathbf{M}_s + \mathbf{R}_d m_d \mathbf{R}_d^T) \mathbf{R}_s \ddot{\mathbf{x}}_g(t) \quad (8) \\ (m_d + b) \dot{y}(t) + (m_d \mathbf{R}_d^T + b \mathbf{R}_c^T) \ddot{\mathbf{x}}_s(t) + c_d \dot{y}(t) + k_d y(t) = -m_d \mathbf{R}_d^T \mathbf{R}_s \ddot{\mathbf{x}}_g(t) \end{aligned}$$

where $\mathbf{R}_d \in \mathbb{R}^n$ and $\mathbf{R}_b \in \mathbb{R}^n$ are the location vectors specifying the floor that the spring/dashpot or inerter are connected to, respectively (vectors of zeros with a single one on its i_d or i_b entry, respectively), and \mathbf{R}_c is defined as $\mathbf{R}_c = \mathbf{R}_d - \mathbf{R}_b$. Note that the forces transferred by the spring/dashpot combination or by the inerter to the host structure, needed later in the design problem formulation, are, respectively:

$$f_d(t) = c_d \dot{y}(t) + k_d y(t) \quad (9)$$

$$f_b(t) = b[\dot{y}(t) + \mathbf{R}_c \ddot{\mathbf{x}}_s(t)] \quad (10)$$

The linear models are established by replacing the hysteretic forces in Eqs. (6) or (8) with the linear ones $\mathbf{K}_s \mathbf{x}_s(t)$. The state space formulation for these linear models, that will be used later to estimate the stationary response statistics, is discussed in Appendix A.

4. Performance quantification

In this work, a bi-objective optimization problem is adopted for the SPD design, to explore the influence of modeling fidelity across a wide range of favorable (Pareto-dominant) configurations for each device. The vibration suppression effectiveness, represented through reduction of engineering demand parameter (EDP) responses, and the size of the device, represented through the control forces exerted to the structure, are used as competing objectives. As EDPs, both inter-story drifts ratios and absolute floor accelerations will be considered. These EDP types may be used to describe, respectively, the performance (fragility) of structural or non-structural components and building contents.

For stationary excitation the response is quantified using the statistics of the stochastic output, while for non-stationary excitation the distribution of peak responses is used for the same task. With respect to the fidelity of the performance quantification, two approaches will be examined: (i) the average response across the EDPs; and (ii) the consequences associated with different damage states, the latter related to the probability of the EDPs exceeding different thresholds. Approach (i) has a different interpretation for each of the two excitation descriptions, as detailed in the next sections. It will be termed as average performance quantification and will be denoted as A . Approach (ii) follows directly modern PBEE standards [71] for quantifying seismic performance, and will be regarded herein as the higher fidelity one. It will be termed as risk-based performance quantification and will be denoted as R . This risk-based characterization has the same foundation independently of the excitation description: it is based on a component-based vulnerability assessment [72] and entails the definition of different damage states and of the consequences associated with each of these damage states.

To formalize the problem formulation let n_e represent the total number of distinct EDPs of interest (across all floors of the structure), with the i th EDP denoted as edp_i . If n_i^d is the number of damage states for the i th EDP and C_i^j are the additional consequences for exceeding the j th threshold compared to the consequences for exceeding the previous ($j-1$) threshold, then the consequences (losses) associated with the i th EDP, L_i , and the total consequences (total losses) across all EDPs, L , are:

$$L_i = \sum_{j=1}^{n_i^d} C_i^j P_i^j; \quad L = \sum_{i=1}^{n_e} L_i = \sum_{i=1}^{n_e} \sum_{j=1}^{n_i^d} C_i^j P_i^j \quad (11)$$

where P_i^j is the probability that the i th EDP will exceed the threshold b_i^j defining its j th damage state. This probability will be quantified using an appropriate context for each type of excitation.

In sections 4.2 and 4.3 details for estimating the aforementioned performance quantifications are discussed, separately for each excitation description. To better frame presentation within the objective functions utilized in the design problem formulation, some details of the design optimization are discussed first.

4.1 General characteristics of the design problem formulation

Let $\boldsymbol{\varphi}$ denote the design variable vector, corresponding to the controllable parameters of each SPD. For the VD implementation, this vector corresponds to the damping coefficients for each of the dampers $\boldsymbol{\varphi} = \{c_i; i=1, \dots, l\}$ whereas for the TMDI implementation this vector is composed of the dimensionless frequency ratio r_d , damping ratio ζ_d , inertance ratio β , and mass ratio μ , leading to $\boldsymbol{\varphi} = \{r_d, \zeta_d, \beta, \mu\}$, with the dimensionless quantities defined as:

$$r_d = \frac{1}{\omega_1} \sqrt{\frac{k_d}{(m_d + b)}}; \quad \zeta_d = \frac{c_d}{2(m_d + b)\omega_d}; \quad \beta = \frac{b}{M}; \quad \mu = \frac{m_d}{M} \quad (12)$$

where M and ω_1 are total mass and the fundamental natural frequency of the host structure respectively. For the TID and TMD, the design is simplified by removing, respectively, μ and β from the $\boldsymbol{\varphi}$ definition.

The first objective $J_1(\boldsymbol{\varphi})$ in the bi-objective optimization represents the structural performance and is expressed through the response statistics for the different EDPs. The second objective $J_2(\boldsymbol{\varphi})$ corresponds to the magnitude of the SPD control forces, and is related to the upfront cost of the device itself [41] or to the local strengthening of the host structure required for the transmission of the SPD forces [35, 46]. For the VDs the sum of all the damper forces will be used to define $J_2(\boldsymbol{\varphi})$, as each of these forces represents device implementation at a different floor, while for the IVA, the maximum between forces f_b and f_d is adopted, following the implementation in [26]. With respect to the specific selection of the second objective, it is important to acknowledge that for some conventional vibration absorbers (including the TMD) a more appropriate device-related performance objective would had been the secondary mass or damper stroke. Nevertheless, for inerter-based vibration absorbers (e.g. TID and TMDI) the presence of the inerter alleviates the need for large secondary mass and reduces dramatically the damper stroke (e.g. [16]), at the expense of large inerter forces. Therefore, for TID/TMDIs the device force becomes the critical objective to minimize (or to examine) as it governs the cost of the device and its connection to the host/primary structure (e.g. [35]). Similar remark holds for VDs, whose cost is related to the damper force (e.g. [27]). These considerations justify the use of SPD force as the second objective in this work to establish meaningful comparisons across all the SPDs.

4.2 Performance quantification for stationary excitation

For the stationary excitation case, the performance quantification is expressed through response statistics obtained through random vibration theory [73]. For the average performance quantification, the second-order (variance) statistics are utilized. This is the typical performance definition for stationary excitation [20, 74], as it leads to analytically tractable solutions [75, 76]. The average structural performance objective (J_1) is therefore defined as:

$$J_A^S(\boldsymbol{\varphi}) = \sum_{i=1}^{n_e} w_i^2 \sigma_{edp_i}^2(\boldsymbol{\varphi}) \quad (13)$$

where $\sigma_{edp_i}^2$ is the variance of output edp_i and w_i is the weight for that output, quantifying its relative importance in the formulation of the overall objective function. Herein subscript will be used to distinguish the performance quantification (average A or risk-based R) and superscripts to distinguish the underlying excitation description (stationary S or non-stationary NS). In the linear control theory literature, measure J_A^S is associated with \mathcal{H}_2 optimal control (when the problem is posed deterministically, in the frequency domain), or as Linear Quadratic Gaussian (LQG) control (when it is posed stochastically) [42]. In the interest of brevity, we also will frequently refer to J_A^S as the \mathcal{H}_2 measure/design. The corresponding definition for the objective function related to control force magnitude (J_2) is:

$$\begin{aligned} \underline{J}_A^S(\boldsymbol{\varphi}) &= \sum_{i=1}^l \sigma_{f_i}(\boldsymbol{\varphi}) \text{ for VD} \\ \underline{J}_A^S(\boldsymbol{\varphi}) &= \max\{\sigma_{f_b}(\boldsymbol{\varphi}), \sigma_{f_d}(\boldsymbol{\varphi})\} \text{ for IVA} \end{aligned} \quad (14)$$

where $\sigma_{f_i}(\boldsymbol{\varphi})$ is the standard deviation of the VD forces, while $\sigma_{f_b}(\boldsymbol{\varphi})$ and $\sigma_{f_d}(\boldsymbol{\varphi})$ are the standard deviation of the forces exerted by the IVA to the host structure (inertor or combination of spring and dashpot, respectively). Herein an underscore $\underline{\quad}$ will be used to distinguish the objectives related to the SPD forces. The estimation of all the variance quantities needed in Eqs. (13) and (14) is discussed in Appendix B for the linear structural model. For the nonlinear, hysteretic structural model, the stationary case does not have an analytically tractable solution apart from special cases, and therefore it is not examined here (nor it is used in typical SPD design), as there is no benefit of utilizing a lower-fidelity approach that does not offer computational advantages.

For the risk-based quantification, probability P_i^j is equal to the first-passage probability $P_i(\boldsymbol{\varphi} | \beta_i^j, T)$ of output edp_i out-crossing threshold b_i^j within duration T ,

$$P_i(\boldsymbol{\varphi} | \beta_i^j, T) = P\left[|edp_i(\tau)| > \beta_i^j \text{ for some } \tau \in [0, T]\right] \quad (15)$$

where T represents the duration of the strong part of the ground motion, for which response can be approximated as stationary. This leads to objective function definition (J_1) for structural performance:

$$J_R^S(\boldsymbol{\varphi}) = \sum_{i=1}^{n_e} \sum_{j=1}^{n_i^d} C_i^j P_i(\boldsymbol{\varphi} | \beta_i^j, T) \quad (16)$$

For the definition for the SPD force objective function (J_2), the use of peak instead of RMS forces is considered, accommodated through the introduction of peak response factors [77]. This leads to:

$$\begin{aligned} \underline{J}_R^S(\boldsymbol{\varphi}) &= \sum_{i=1}^l p_{f_i}(\boldsymbol{\varphi}, T) \sigma_{f_i}(\boldsymbol{\varphi}) \text{ for VD} \\ \underline{J}_R^S(\boldsymbol{\varphi}) &= \max \left\{ p_{f_b}(\boldsymbol{\varphi}, T) \sigma_{f_b}(\boldsymbol{\varphi}), p_{f_d}(\boldsymbol{\varphi}, T) \sigma_{f_d}(\boldsymbol{\varphi}) \right\} \text{ for IVA} \end{aligned} \quad (17)$$

where $p_{f_i}(\boldsymbol{\varphi}, T)$ is peak factor for the VD forces for duration T , while $p_{f_b}(\boldsymbol{\varphi}, T)$ and $p_{f_d}(\boldsymbol{\varphi}, T)$ are peak factors for the forces exerted by the IVA to the host structure, again for duration T . Estimation of the first-passage probabilities and the peak factors is also discussed in Appendix B. Note that the use of peak forces instead of the RMS forces is more appropriate to describe magnitude of SPD forces in general, but when the \mathcal{H}_2 (average) formulation is adopted for the structural performance objective, the RMS quantification is preferred since it is numerically easier to estimate (similar complexity as the estimation of the $J_A^S(\boldsymbol{\varphi})$ objective), and is independent of the assumed duration T . Estimation of the peak forces, entails a higher computational burden, since it involves additionally the estimation of the peak factors, requiring estimation of bandwidth parameters as detailed in Appendix B. Overall, for the stationary excitation description the risk-based performance quantification involves a moderately larger burden due to the requirement to estimate these bandwidth parameters.

4.3 Performance quantification for non-stationary excitation

For the non-stationary excitation case, all performance quantifications are based on peak responses over the excitation duration. The relevant statistics are obtained adopting a Monte Carlo approach, using realizations (samples) of the earthquake acceleration ground motions, obtained through the process detailed

in Section 2.2. This way for both the NS and NS_r descriptions, a discrete number of ground motions is utilized to characterize the seismic excitation. Simply the way these ground motions are created differs: through samples from the stochastic ground motion model for NS , and through selection of compatible recorded ground motions for NS_r .

For the average performance quantification, the geometric mean of the peak response is used. Note that the geometric mean instead of the mean is utilized for consistency with modern PBEE practices that assume lognormal EDP distribution [71, 78, 79], for which the geometric mean represents the median EDP. Let $edp_i^h(\boldsymbol{\varphi})$ denote the peak value for the i th EDP for the h th ground motion $\ddot{x}_g^h(t)$, and assume that n_h ground motions are used to describe the seismic excitation. The geometric mean of the EDP, $\overline{edp}_i(\boldsymbol{\varphi})$, based on the samples $\{edp_i^h(\boldsymbol{\varphi}); i = 1, \dots, n_h\}$ is given by:

$$\overline{edp}_i(\boldsymbol{\varphi}) = \sqrt[n_h]{\prod_{h=1}^{n_h} edp_i^h(\boldsymbol{\varphi})} \quad (18)$$

The average structural performance objective (J_1) is subsequently defined as:

$$J_A^{NS}(\boldsymbol{\varphi}) = \sum_{i=1}^{n_e} w_i \overline{edp}_i(\boldsymbol{\varphi}) \quad (19)$$

The corresponding definition for the objective function related to control force magnitude (J_2) is:

$$\begin{aligned} \underline{J}^{NS}(\boldsymbol{\varphi}) &= \sum_{i=1}^l \overline{f}_i(\boldsymbol{\varphi}) \text{ for VD} \\ \underline{J}^{NS}(\boldsymbol{\varphi}) &= \max\{\overline{f}_b(\boldsymbol{\varphi}), \overline{f}_d(\boldsymbol{\varphi})\} \text{ for IVA} \end{aligned} \quad (20)$$

where $\overline{f}_i(\boldsymbol{\varphi})$ is the geometric mean of the peak VD forces, while $\overline{f}_b(\boldsymbol{\varphi})$ and $\overline{f}_d(\boldsymbol{\varphi})$ are the geometric mean of the peak forces exerted by the IVA to the host structure. These geometric mean statistics are calculated using an expression similar to Eq. (18), by replacing the peak EDP responses for each excitation with the peak SPD force responses.

For the risk-based quantification, probability P_i^j is expressed through the empirical distribution based on the available samples, $\{edp_i^h(\boldsymbol{\varphi}); i=1, \dots, n_h\}$, leading to quantification as:

$$P_i(edp_i(\boldsymbol{\varphi}) > \beta_i^j) = \frac{1}{n_h} \sum_{h=1}^{n_h} I[(edp_i^h(\boldsymbol{\varphi}) > \beta_i^j)] \quad (21)$$

where $I[\cdot]$ is the indicator function, corresponding to 1 if the relationship between the brackets is satisfied, or 0 otherwise. This leads to objective function definition (J_1) for structural performance:

$$J_R^{NS}(\boldsymbol{\varphi}) = \sum_{i=1}^{n_e} \sum_{j=1}^{n_i^d} C_i^j \frac{1}{n_h} \sum_{h=1}^{n_h} I[(edp_i^h(\boldsymbol{\varphi}) > \beta_i^j)] \quad (22)$$

For the risk-based SPD force objective function (J_1), an identical definition to the one utilized for the average performance quantification, given by Eq. (20), is adopted. Thus, the notation for the objective function in Eq. (20) does not indicate a dependence on the type of performance quantification, i.e. subscript is missing, since it is chosen common across both the average and the risk-based quantifications.

Notably, for the non-stationary excitation description, the different performance quantification models have the same computational burden, since they both utilize the same responses over the ground motion ensemble $\{\ddot{x}_g^h; i=1, \dots, n_h\}$.

5. Details for the SPD bi-objective design problem

5.1 Design problem formulation and solution

As detailed in section 4.1, the bi-objective design problem is established by considering two competing objectives

$$\boldsymbol{\varphi}^* = \arg \min_{\boldsymbol{\varphi} \in \Phi_d} \{J_1(\boldsymbol{\varphi}), J_2(\boldsymbol{\varphi})\} \quad (23)$$

where Φ_d represents the admissible design space for the design variable vector $\boldsymbol{\varphi}$, and the details for the two objective function selection depend on the model fidelity assumption. The latter, and the definition of

the corresponding design variants are discussed in detail in Section 5.2. Solution of the multi-objective problem is facilitated through the identification of the dominant designs, representing the Pareto optimal solutions across the two competing objectives. A SPD design $\boldsymbol{\varphi}$ is defined as dominant (Pareto optimal), and denoted as $\boldsymbol{\varphi}_p$, if there exist no other design configuration that can simultaneously improve both objectives (i.e. improvement of one objective can only come with detriment to the other). The set of all such configurations is defined as the Pareto set Φ_p , whereas the representation of this set in the objective function space is defined as the Pareto front J_p . This Pareto front reveals the compromises that can be achieved for the two competing objectives across the different SPD configurations, and in the context of this study accommodates comparisons of the model-fidelity impact across a wide range of favorable (dominant) configurations.

For solving the bi-objective optimization problem, the random search optimization scheme [80] proposed in [38] is adopted, as it can facilitate efficient identification of the Pareto front for different performance characterization choices. This solution scheme involves the following steps. Initially a large population of N_c candidate design configurations are generated within Φ_d , $\{\boldsymbol{\varphi}^{(c)}; c=1, \dots, N_c\}$, adopting Latin Hypercube (i.e. space filling) sampling, with N_c chosen large enough to ensure adequate density within the entire search domain. The response is subsequently estimated for all the candidate design configurations. Finally, selection of the type of performance quantification and of the weights $\{w_i; i=1, \dots, n_e\}$ (for A) or of the details $\{\beta_i^j, C_i^j; j=1, \dots, n_i^d\}$ (for R) are chosen to estimate the competing objectives for the candidate set $\{J_1(\boldsymbol{\varphi}^{(c)}), J_2(\boldsymbol{\varphi}^{(c)}); c=1, \dots, N_c\}$ and, ultimately, the identification of the dominant designs within this set and the Pareto front. For different design problems formulations corresponding to different selections of the performance quantification and of the corresponding characteristics $\{w_i; i=1, \dots, n_e\}$ or $\{\beta_i^j, C_i^j; j=1, \dots, n_i^d\}$, the first two computationally expensive steps of the numerical optimization do not need to be repeated, accommodating high efficiency in the Pareto front identification.

5.2 Variants of the design problem based on model fidelity

Combining the different models for the excitation, structural response and performance quantification, different variants of the design problem are defined as follows (also reviewed in Table 1):

- $D_{A,L}^S$: average performance for stationary excitation and linear response, which adopts $J_A^S(\boldsymbol{\varphi})$ of Eq. (13) as J_1 and $\underline{J}_A^S(\boldsymbol{\varphi})$ of Eq. (14) as J_2 .
- $D_{R,L}^S$: risk-based performance for stationary excitation and linear response, which adopts $J_R^S(\boldsymbol{\varphi})$ of Eq. (16) as J_1 and $\underline{J}_R^S(\boldsymbol{\varphi})$ of Eq. (17) as J_2 .
- $D_{A,L}^{NS}$: average performance for non-stationary excitation using a stochastic ground motion model and linear response, which adopts $J_A^{NS}(\boldsymbol{\varphi})$ of Eq. (19) as J_1 and $\underline{J}^{NS}(\boldsymbol{\varphi})$ of Eq. (20) as J_2 . In this case, the ground motion ensemble $\{\ddot{x}_g^h; i=1, \dots, n_h\}$ is obtained through a stochastic ground motion model.
- $D_{R,L}^{NS}$: risk-based performance for non-stationary excitation using a stochastic ground motion model and linear response, which adopts $J_R^{NS}(\boldsymbol{\varphi})$ of Eq. (22) as J_1 and $\underline{J}^{NS}(\boldsymbol{\varphi})$ of Eq. (20) as J_2 . In this case, the ground motion ensemble $\{\ddot{x}_g^h; i=1, \dots, n_h\}$ is obtained through a stochastic ground motion model.
- $D_{A,L}^{NS_r}$, $D_{R,L}^{NS_r}$: identical to $D_{A,L}^{NS}$ and $D_{R,L}^{NS}$, respectively with only difference that ground motion ensemble $\{\ddot{x}_g^h; i=1, \dots, n_h\}$ is obtained through selection and scaling of ground motions.
- $D_{A,NL}^{NS}$, $D_{R,NL}^{NS}$, $D_{A,NL}^{NS_r}$, $D_{R,NL}^{NS_r}$: identical to $D_{A,L}^{NS}$, $D_{R,L}^{NS}$, $D_{A,L}^{NS_r}$ and $D_{R,L}^{NS_r}$, respectively, with only difference that nonlinear model is used instead of a linear one.

With respect to the computational burden of the different approaches, small differences exist between the different performance quantifications (or no differences in the case of non-stationary excitation description). However, the non-stationary excitation description involves substantially higher computational cost compared to the use of the stationary excitation description, for which tractable semi-

analytical solutions exist with no requirement to perform time-history analysis. The use of nonlinear structural models, compared to linear models, further increases computational cost even when a reduced-order formulation is adopted. The computational burden for all designs that involve a non-stationary excitation description is proportional to the number of ground motions n_h used to describe the seismic hazard. To investigate the influence of this selection on the optimal design, a simplified variant of some of the designs that involve non-stationary excitation description is also examined, using a small number of only $n_h=7$ sample excitations. This number of ground motions is considered as the minimum number of excitations to allow for structural design based on average peak inelastic demands in most international seismic design codes of practice [81]. Similar number of ground motions has been used in past studies examining PBEE and/or SPD design [38, 82]. This design variant will be distinguished by adding notation \sim over D , and will be considered only for the NS_r excitation description.

Table 1: Summary of notation used to describe the different modeling fidelity and design approaches

| | |
|---------------|--|
| S, NS, NS_r | Earthquake excitation model: Stationary model (S); Non-stationary model with ground motions obtained through a stochastic ground motion model (NS); Non-stationary model with ground motions obtained through selection and scaling of ground motions; |
| L, NL | Structural response model: Linear model (L); Nonlinear model (NL) |
| A, R | Performance quantification model: Average performance (A); Risk-based performance definition (R) |
| J_1, J_2 | General description of objectives for structural response (J_1) or control force (J_2) |
| $T_{c,b}^a$ | Design (if T is D), performance objectives (if T is PO), objective for structural response (if T is J), and objective for control force (if T is \underline{J}): using a seismic excitation description, b model for structural response and c approach for quantifying performance. Subscript b might not necessarily appear for all cases of T . |

6. Illustrative case study: Description

6.1 Structural model and details of SPD implementation

For the case study, two benchmark buildings [83] are considered, corresponding to a three- (denoted as B_1) and nine-story (denoted as B_2) steel moment-resisting frames (MRFs), having fundamental periods of 1.02 s and 2.27 s, respectively. Damping matrix C_s for both structures is modeled through a Rayleigh model, with damping ratios selected as 2% for 1st and 3rd modes. The nonlinear FEMs are developed in OpenSees using fiber modeling approach for describing the hysteretic behavior. Details for the OpenSees models and for the ROM formulation are discussed in [45]. It is important to acknowledge that the chosen damping ratio will impact the relevant effectiveness of the SPDs, with larger values for it leading to smaller levels of vibration suppression compared to the unprotected structure. This might possibly impact some of the identified later trends, for example trends associated with nonlinear behavior, since the magnitude of this behavior might be reduced due to the higher inherent structural damping. Examining the impact of the damping ratio on these trends falls outside the scope of this paper, though, since the emphasis is on the modeling fidelity assumptions (and not the building model assumptions). Furthermore, the impact of the chosen damping ratio in the study is expected to be small since across all aspects of design and assessment (including selection of excitation intensity), the actual damping ratio is explicitly considered.

For the VD implementation, for both structures placement of dampers in each floor is considered, leading to $l=3$ for structure B_1 and $l=9$ for structure B_2 . For structure B_1 , the coefficient c_i for the dampers for each floor are independently chosen, while for structure B_2 , same damping coefficient is considered for the dampers of the first three stories, the next three stories and the final three stories, leading to three group of dampers with same damping coefficient. For the IVA implementation, for structure B_1 , configuration $i_d=3$ and $i_b=2$ is examined (mass connected at top floor and inerter connected to the floor below), while for structure B_2 , configuration $i_d=8$ and $i_b=7$ is examined (mass connected at second from the top floor and inerter connected to the floor below). The specific placement for the B_2 structure is chosen to improve efficiency of the TMDI/TID applications. Extensive discussions on the impact of the IVA placement on its

efficiency can be found in [24, 26, 35], thus further investigation of this topic falls out of the scope of the present study.

6.2 Excitation models

The parameters of the envelop function $e_i(t)$ of Eq. (3) for the stochastic ground motion model description are selected as $T_r=15$ s, $T_p=20$ s and α chosen so that the envelope value is 0.05 for $t=60$ s. This leads to ground motion with significant duration $D_{5-95}=24$ s. The parameters of $S_g(\omega)$ are chosen so that the response spectrum derived from the NS excitation description (using the aforementioned envelope) has minimized discrepancy to the design spectrum for the two structures, which is the UBC 1994 spectrum [83]. This leads to values $\omega_g=4.49\pi$, $\zeta_g=0.75$, $\omega_f=0.48\pi$, $\zeta_f=0.8$, and $a_{RMS}=0.14g$. The NS_r ground motions are selected from the PEER NGA-West ground motion database within a range of significant duration centered around 24 s (range from 22 s to 26 s), to be compatible with the stochastic ground motion model description, and are appropriately scaled so that the MSE between response spectrum derived from the selected ground motions and the design spectrum of the two structures is minimized. To illustrate the overall compatibility of the ground motion modeling approaches, Fig. 2 shows (i) the UBC 1994 design spectrum, (ii) the spectrum obtained by the stochastic ground motion model (NS excitation) with the aforementioned parameters, and (iii) spectrum obtained by the chosen ground motions (NS_r excitation) for structure B_1 . In both (ii) and (iii), the dispersion (variability) of the responses is also shown to facilitate some of the discussions in the next section. Results show that good average compatibility is achieved, while the NS_r excitation description provides larger spectral response dispersion than the NS excitation description. This should be attributed to the fact that the non-stationary stochastic ground motion modeling approach adopted here, with excitation variability attributed only to the stochastic white noise sequence, is expected [56] to under predict the dispersion of the response compared to the dispersion observed in recorder ground motions.

The number of ground motion samples is chosen as $n_h=100$ s for NS and $n_h=60$ for NS_r . The lower value for NS_r was necessitated by the constraint placed on the ground motion selection, such as the significant

duration but most importantly the scaling factor that had to be less or equal to 3, to avoid bias in the calculated structural response introduced by larger values for this scaling factor [61, 84]. For the risk-based quantification for the stationary excitation description, the duration T is taken equal to the duration of the plateau of the envelop function T_2 , to promote further consistency of the comparisons.

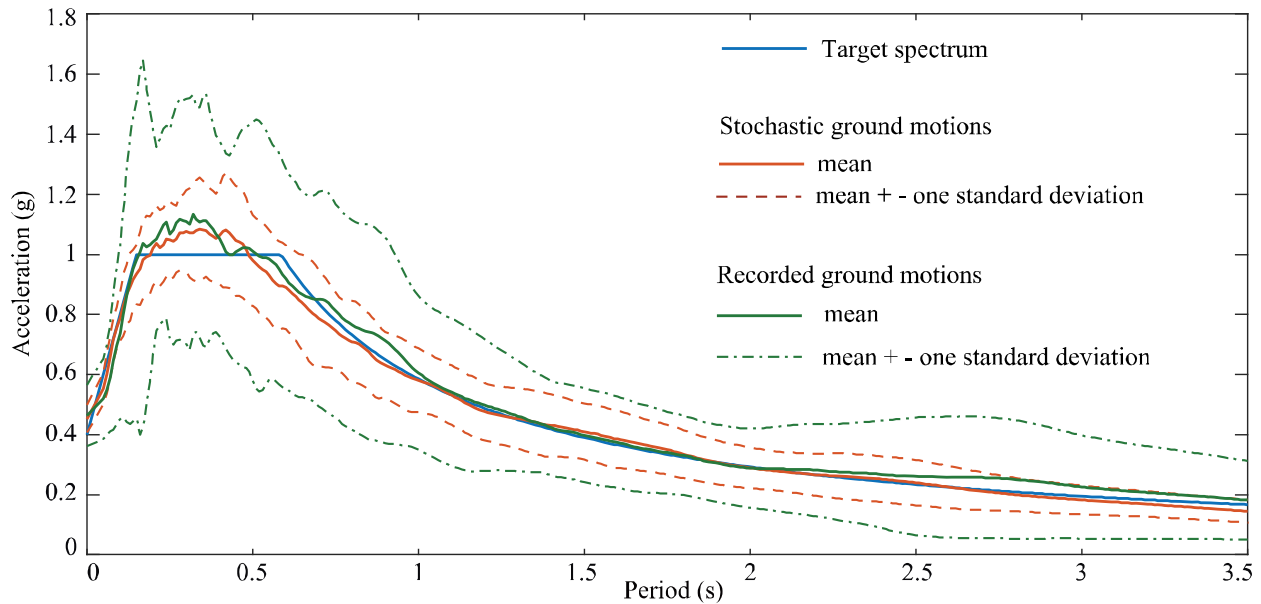


Fig. 2: Comparison of UBC 1994 design spectrum to spectrum established by the NS and NS_r (for structure B_1) excitation descriptions.

6.3 Performance quantification

For the risk-based quantification, the pair $\{\beta_i^j, C_i^j; j = 1, \dots, n_i^d\}$ is taken to be the same across all floors. For both EDPs, three damage states are established ($n_i^d = 3$), corresponding to light ($j=1$), moderate ($j=2$) and severe ($j=3$) damage. The values of the damage thresholds, along with their corresponding consequences are presented in Table 2. All represent typical values adopted for PBEE applications [65], with consequences taken to represent repair cost. Note that only the relative ratio of the consequences impacts the optimal design due to the linear relationship to objective J_1 . For this reason, most results for objective J_1 will be presented normalized by the value of objective J_1 for the uncontrolled structure. This will also be adopted for the average performance quantification to accommodate easier comparisons across the different designs. For the average performance quantifications, the weights w_i are taken equal to the

reciprocal damage thresholds for the last damage state β_i^3 , to accommodate some compatibility between the two alternative performance quantifications.

Furthermore, three different cases are examined for the definition of J_1 , providing different importance to drift and acceleration EDPs: (1) the first one, denoted as O_1 , considers only the inter-storey drifts as EDPs and is referenced hereafter as a drift-sensitive design; (2) the second one, denoted as O_2 , includes only the absolute floor accelerations as EDPs, referenced hereafter as an acceleration-sensitive design; (3) the third one, denoted as O_3 , includes both inter-storey drift ratios and accelerations and is referenced as balanced design. The drift-sensitive and acceleration-sensitive designs are accommodated by setting C_i^j (for R performance quantification) or weights w_i (for A performance quantification) equal to zero for the other type of EDP. The recommended implementation is O_3 , formulating performance through the contribution of all EDP types, and the two other ones are examined to reveal any trends that are specific to drift (for O_1) or acceleration (for O_2) mitigation. As discussed in Section 5.1, leveraging the random search approach, the optimal configurations and performance for the drift-sensitive and acceleration-sensitive designs is obtained for the same computational burden that is needed for the nominal design case, the balanced design.

Notation D is used to denote design, as discussed in Section 5.2, and notation PO is used to indicate performance objectives, following same subscript and superscript meaning as for D as indicated also in Table 1. Note that for all design D , the performance objective PO can be evaluated across different assumptions, for example evaluate risk-based performance objectives for designs that utilized average performance quantification for the objective function definition (used to identify these designs). This is how the implications of model fidelity will be ultimately examined. The total number of variants, considering all the possible combinations for structural behavior, seismic excitation and performance quantification are 35 for each structure and SPD implementation, though only specific combinations, resulting in interesting comparisons, will be presented in detail.

Table 2: Performance threshold and consequence values for the risk-based performance quantification. Values are taken to be the same across all floors.

| Fragility function values | damage thresholds β_i^j | | | Consequences C_i^j | | |
|------------------------------|-------------------------------|-------|-------|----------------------|-----------|-----------|
| | $j=1$ | $j=2$ | $j=3$ | $j=1$ | $j=2$ | $j=3$ |
| Inter-story drifts ratios | 0.21% | 1.2% | 2.5% | \$31,000 | \$200,000 | \$300,000 |
| Absolute floor accelerations | 0.4g | 0.6g | 1.0g | \$25,000 | \$60,000 | \$246,000 |

6.4 Design optimization details

For the VD implementation, the admissible space of the optimization problem is defined so that supplemental damping up to 50% is achieved through the addition of the viscous dampers in the linear structure, considering a uniform damper distribution. Note that this uniform distribution is only utilized for the admissible space definition, and the actual damper configuration may have non-uniform height-distribution characteristics. For the IVA implementation, the admissible space of the optimization problem is taken to be $[0.01 \ 2]$ for r_d , $[0.005 \ 1.5]$ for ζ_d , $[0 \ 6]$ for β and $[0 \ 0.05]$ for μ . The lower bound of the range for the mass and inertance ratios are chosen as zero in order to examine TID and TMD configurations, respectively, additionally to the most general TMDI configuration. The upper bound of the mass ratio is selected to accommodate a mass damper that does not excessively increase gravity loads of the host structure. The lower and upper bounds of the remaining design variables are chosen to avoid convergence to their respective boundaries, while also avoiding unrealistically large inertance values. The total number of candidate design configurations N_c , is chosen large (400,000 for each SPD implementation) to ensure an accurate identification of the Pareto front. This is made possible through the computational efficiency supported by the ROM framework. In order to simplify presentation of the results, a selective set of 35 designs is typically chosen to represent the Pareto front, even though a larger number of dominant designs is identified. Note that the fact that a large population of dominant designs is identified, as also shown in some of the presented results, verifies that the selection of N_c is appropriate.

7. Illustrative case study: Results and comparisons

The impact of model fidelity is numerically quantified by examining the deviation of performance objectives, J , achieved by different optimal SPD designs ϕ due to variation of the modelling assumptions fidelity. The reason for focusing solely on differences to the performance objectives without examining optimal SPD design parameters ϕ is that, even though differences in ϕ can provide some insights, they do not necessarily indicate performance inconsistencies due to (poor) modelling assumption in the SPD design. This is because correlations between the design variables, as well as low sensitivity with respect to some ϕ components for some of the objectives, may ultimately yield similar performance for different design vectors ϕ . In this respect, attention is herein focused on comparing performance objectives achieved by designs that use simplified, lower-fidelity, assumptions vis-a-vis the actual Pareto optimal performance derived from the SPD design that adopts the desired objective quantification. These comparisons enable the identification and quantification of a potential suboptimality of the lower fidelity design assumptions by addressing the fundamental question: what is the reduction of the SPD efficiency if the design is performed using simplistic performance objectives (to accommodate an easier design optimization) compared to the quantification that describes the actual performance objectives of our structure (actual Pareto front)? Moreover, comparisons using performance objectives based on different modelling assumptions will ultimately provide answers about the robustness of each of the SPD design variants.

Since the number of fidelity assumptions for describing performance objectives and the number of potential design variants is substantial, it is impractical to perform exhaustive comparisons. Instead our focus is only on realistic implementations, increasing gradually the fidelity of the performance objectives and comparing against alternative design variants that are compatible in the model hierarchy (use similar modeling assumptions as the performance objectives considered) or that one would consider in practical settings. As mentioned above, the performance for these alternative design variants is compared against the actual Pareto front, the one established by the design variant that uses the same modeling assumptions as the performance objectives examined. Since response to actual earthquakes is non-stationary, and modern

Patsialis D, Taflanidis AA, Giaralis A (2023) Exploring the impact of excitation and structural response/performance modeling fidelity in the design of seismic protective devices. *Engineering Structures*, Accepted 13/2/2023.

PBEE standards emphasize risk-based performance quantifications, the basis of our comparisons is typically R performance and NS/NS_r excitation. On the other hand, since design of SPDs is very commonly performed using an assumption for stationary excitation, comparison to the performance objectives of the designs obtained using the simplified S excitation description will be considered in most of the cases examined. Beyond these simplistic design variants corresponding to S stationary description, design variant alternatives that are closely related to the performance objectives examined in each case, will be also considered, as detailed later on.

Before dwelling on these comparisons, it is deemed informative to first quantify and discuss pairwise correlations between related performance objectives, presented in the next subsection.

7.1 Comparison across related pairs of various performance objectives

Comparisons across pairs of related performance objectives are established within the considered model fidelity hierarchy in Fig. 3 for VD implementation and in Fig. 4 for IVA implementation. Results pertain to the 3-storey (B_1) benchmark structure and for the balanced SPD design (O_3) accounting for both storey-drifts and floor accelerations EDPs. Panels of plots in each of the two figures are organized such that the performance objectives in the x-axis are the same for both rows of panels. The first two panels compare stationary (S) versus stochastic non-stationary (NS) excitation descriptions [(a): $J_{R,L}^S$ vs $J_{R,L}^{NS}$ and (b): $\underline{J}_{R,L}^S$ vs $\underline{J}_{R,L}^{NS}$]. The next two panels compare linear (L) versus nonlinear (NL) response [(c): $J_{R,L}^{NS}$ vs $J_{R,NL}^{NS}$ and (d): $J_{A,NL}^{NS}$ vs $J_{A,L}^{NS}$]. The lower row of panels compare stochastic non-stationary excitation modelling (NS) versus recorded non-stationary excitation modelling (NS_r) [(e): $J_{R,L}^{NS_r}$ vs $J_{R,L}^{NS}$, (f): $\underline{J}_{R,L}^{NS_r}$ vs $\underline{J}_{R,L}^{NS}$, (g): $J_{R,NL}^{NS_r}$ vs $J_{R,NL}^{NS}$ and (h): $J_{A,L}^{NS_r}$ vs $J_{A,L}^{NS}$]. Each of the cases offer further comparisons across other modeling assumptions of interest, since the objectives examined represent a mix of R and A quantifications for either the building performance or the control force. On each plot, the 1:1 line indicating perfect agreement between the two compared performance objectives is drawn, and the correlation coefficient between the objectives, cc , is

reported. The plots include results for configurations identified as Pareto optimal for any of the respective design variants (adopting the compared objectives).

The plotted data in Figs. 3 and 4 reveal an exceptionally high correlation between S and NS risk [Figs. 3 and 4 (a)] and peak response [Figs. 3 and 4 (b)] objectives, as well as between NS and NS_r types of non-stationary excitation modelling for average performance quantification A [Figs. 2 and 4 (f) and (h)]. This high correlation is a preliminary indication that the corresponding optimal designs should be achieving comparable behavior. On the other hand, discrepancies exist between L and NL structural response [Figs. 3 and 4 (c) and (d)], with trends that differ between the two different classes of devices. In particular, for VD (Fig. 3) one can identify a single trend curve that eventually converges to the 1:1 line, with convergence achieved for larger dampers that provide substantial vibration suppression and, therefore, enforce linear response even for the nonlinear structural model. For IVA, multiple trend curves are observed, attributed to the fundamentally different behavior of the different type of devices that are collectively examined under the IVA umbrella (TMDs, TMDIs and TIDs). These differences in the behavior of different IVAs reflect on the Pareto-optimal designs, a topic examined in detail later in subsection 7.3. Moreover, differences are also observed between the risk performance quantification for the NS and NS_r excitation descriptions [Fig. 3 and 4 (e) and (g)]. The similarities for the average performance quantification identified earlier but divergence for risk performance quantification between these two excitation descriptions should be attributed to the fact that the NS excitation provides smaller response dispersion compared to the NS_r excitation, as shown in Fig. 2. Even though considerable consistency is achieved for the median behavior across the two excitation models, the differences between them in the response dispersion lead to differences in the risk objectives, and in particular to an underestimation of risk for the approach with the lower dispersion (NS excitation description). Note that it is well established that the PBEE-based approach utilized for the risk-based performance quantification is impacted by both the median and the dispersion of the structural response [71]. Further, the aforementioned dispersion differences also contribute to larger discrepancies for larger values of median peak control forces [Fig. 3 and 4 (f)], with NS_r yielding larger

force demands, perhaps due to increase of extreme velocity and acceleration responses (based on the larger dispersion) that dictate the magnitude of these forces.

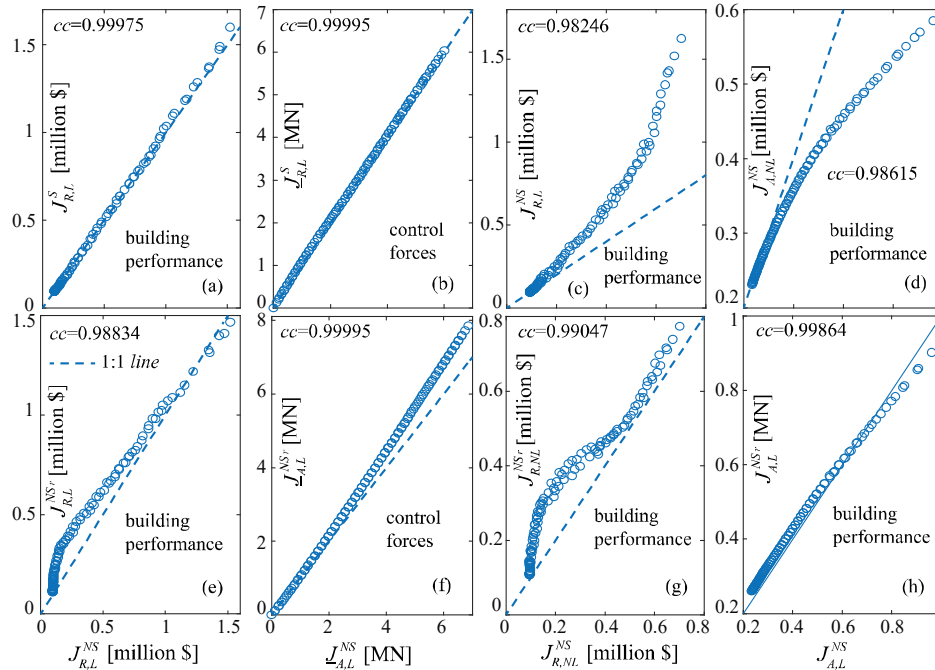


Fig. 3: Comparison of pairs of related performance objectives for structure B_1 and VD device, for balanced (O_2) consequence quantification. Correlation coefficient of the pairs is also displayed. Second row offers comparisons between NS and NS_r excitations while first row between NS and S excitations or L and NL behavior.

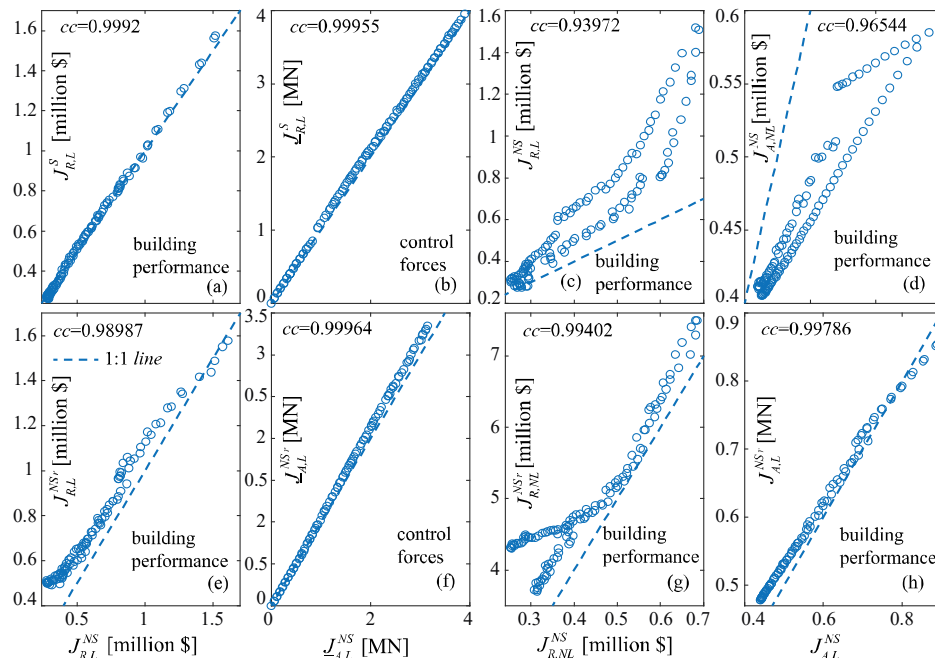


Fig. 4: Comparison of pairs of related performance objectives for structure B_1 and IVA device, for balanced (O_3) consequence quantification. Correlation coefficient of the pairs is also displayed. Second row offers comparisons between NS and NS_r excitations while first row between NS and S excitations or L and NL behavior.

It is important to note that the lower correlation in some of the comparisons in Figs. 3 and 4 does not indicate on its own that the respective optimal designs would yield different behaviors. However, low correlation values do provide a first indication that differences between the designs may exist. Such differences, though, can be only identified if the performance achieved by the different designs is directly compared across the entire Pareto front. These comparisons are presented next.

7.2 Comparison of performance for different design approaches

Comparisons initially examine both benchmark buildings and both classes of SPDs (VDs and IVAs) for the balanced consequence quantification (O_3). Section 7.3 will place some additional emphasis on IVAs, section 7.4. will briefly examine the influence of the number of ground motions used in NS_r , while section 7.5 will discuss selective results for the drift and acceleration sensitive consequence quantifications. In all the plots the building performance objective $J_1(\boldsymbol{\varphi})$ is normalized by the performance of the uncontrolled structure $J_1(0)$, so that the provided objective J_1 corresponds to the reduction when compared against the uncontrolled structure. Discussions here focus on the identification of general trends. A summary of these trends is provided in the conclusion Section 8. For following easier the result presentation, recall that the notation for describing the different variants is summarized in Table 1.

Fig. 5 presents results for both structures and SPDs for objectives corresponding to L response, NS excitation for R performance quantification. The actual Pareto front is compared to lower fidelity designs that use S excitation or A performance quantification. Comparing first the trends between the different devices and buildings, it is evident that for VD more consistent behavior is established across the different design variants. This should be attributed to the difference between the two classes of SPD implementations as well as to the fact that for the IVA implementation, a single device is considered while for the VD implementation, devices are placed at each floor, following the application standards that are common for each SPD class. For this reason, bigger discrepancies are observed for B_2 structure and for IVA implementation; the larger number of stories and the more influential higher mode dynamics for this structure reduce the relative effectiveness of the single IVA device, and make the details of the SPD design

Patsialis D, Taflanidis AA, Giaralis A (2023) Exploring the impact of excitation and structural response/performance modeling fidelity in the design of seismic protective devices. *Engineering Structures*, Accepted 13/2/2023.

more important. This discussion also showcases that results presented here should not be used to compare across the different SPDs and structures, rather only compare the different design variants for the same building and SPD type. The consideration of different structures and protective devices is made to accommodate more comprehensive comparisons and examine what trends for the performance of the different design variants are generalizable. Furthermore, note that the observed performance trends across the buildings and SPDs are actually expected: IVA implementation for the structure B_2 is expected to provide smaller vibration suppression (as indicated by the lower J_1 values) due to the challenges in controlling multiple floors and modes with a single device; the control forces exerted by the SPDs for structure B_2 are expected to be larger due to the larger size of this structure; VDs are expected to offer greater protection (bigger reduction of J_1 for similar levels of J_2) since they correspond to a distributed implementation, with protection devices placed across multiple floors. Should be noted that the latter pattern does not indicate superiority of VDs to IVAs since beyond the magnitude of the control forces, which indeed is an indication of the device cost [35, 41], one needs to consider the total cost of the device implementation which will have additional contributions, for example related to the requirement to accommodate placement of VDs in multiple floors.

Focusing on the comparison between the different design variants, small differences are observed for the VDs, indicating robustness of the respective design approaches, but larger differences for the IVAs, especially for structure B_2 . For the IVAs, the observed trends are also influenced by the fundamental differences between the three different devices represented in this implementation, TMD, TMDI and TID. Though these differences will be explored in detail in the next section by examining the Pareto optimal performance separately for each of them, some preliminary observations can be made here, utilizing trends previously reported in the literature. Specifically, though TMDI and TID are known to yield similar optimal performance when properly designed [26, 38], TMDs have in general smaller effectiveness (larger J_1 values) but also substantially smaller forces (smaller J_2 values). These attributes are manifested as vertical jumps in the Pareto front when moving from dominance of TMD to dominance of TID/TMDI

Patsialis D, Taflanidis AA, Giaralis A (2023) Exploring the impact of excitation and structural response/performance modeling fidelity in the design of seismic protective devices. *Engineering Structures*, Accepted 13/2/2023.

configurations [38]. This is clearly shown in the structure B_2 plots by the vertical jump of the blue circles, representing the actual Pareto front. A similar jump is not observable for structure B_1 because for this shorter and stiffer structure the TMD designs never dominate the TID/TMDI implementations. Additionally, when examining the performance objectives achieved by different design variants, different behaviors are observed between TIDs and TMDIs. This is manifested in Fig. 5(d) as disjoint behavior between two different clusters of the x designs (for stationary, risk-based design variant) corresponding to TMDI and TID implementations for structure B_2 . All these discussions also stress the advantages of examining the impact of the fidelity assumption on the SPD design using a multi-objective setting, as it accommodates comprehensive comparisons across diverse ranges of efficiency for each device, instead of examining these assumptions under a single only definition of optimality.

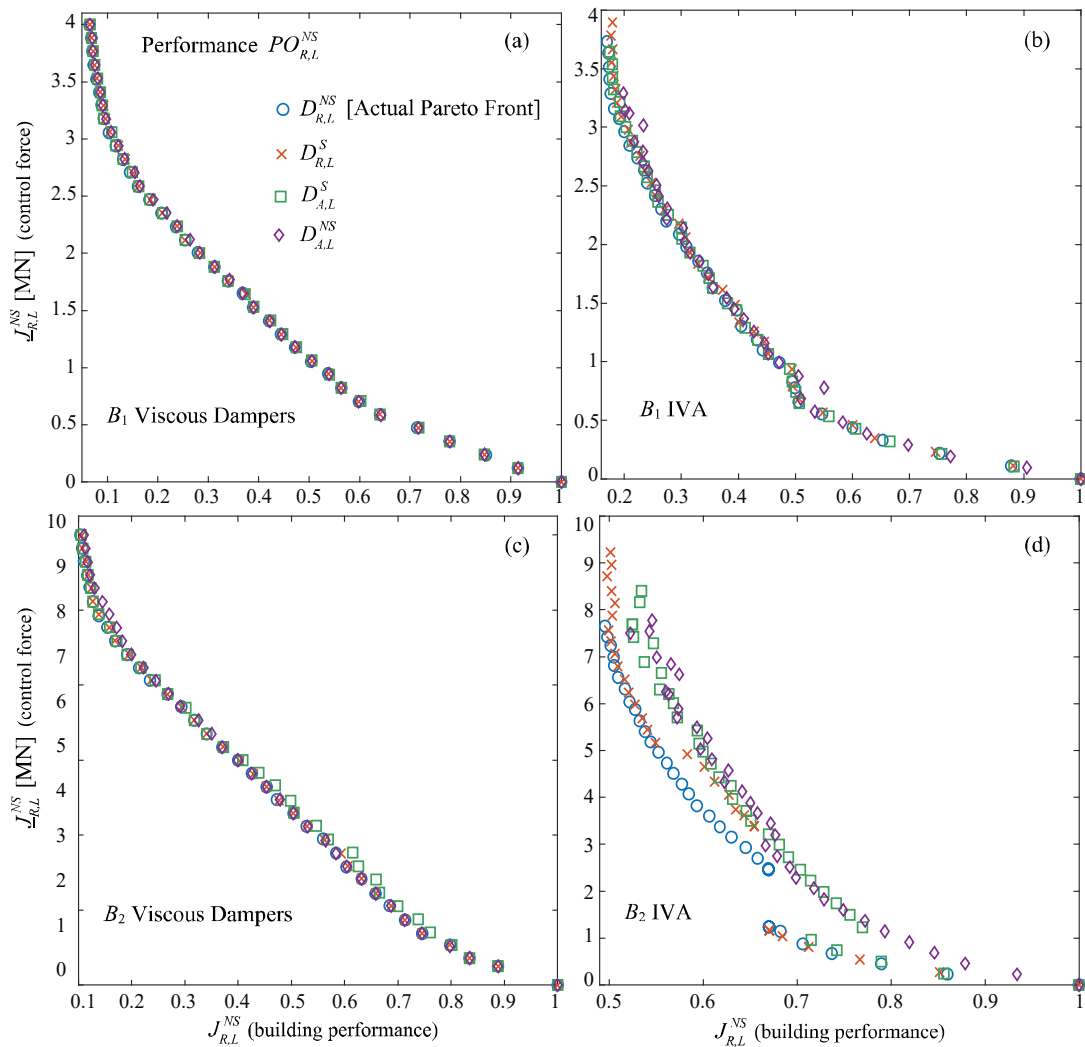


Fig. 5: Risk-based performance assessment for both structures (B_1 and B_2) and SPDs (VD and IVA), for linear structural response model and non-stationary excitation description, for balanced (O_3) consequence quantification. Optimal pareto fronts are compared to the performance objectives achieved using different design variants (stationary and non-stationary) and performance quantifications (risk and average quantifications).

To better focus the comparisons between the different design variants, the next figures examine a specific device and structure. Fig. 6 presents results for structure B_2 and VD implementation, Fig. 7 for structure B_2 and IVA implementation and Fig. 8 for structure B_1 and IVA implementation. Results for structure B_1 and VD implementation are identical to the ones for the same device type for structure B_2 , and are not separately shown hereinafter due to space limitations. In each figure, assessment for different objectives is presented, considering both linear or nonlinear responses, both NS or NS_r excitation description, and for both risk or average performance quantifications. The actual Pareto front in each case

is compared against the performance objectives achieved by compatible, simpler design variants. As such compatible design variants, alternative formulations that adopt a lower fidelity assumption for one of the three modeling aspects (excitation, structural response or performance quantification) while keeping the other two identical are examined: when performance objectives correspond to nonlinear structural response (NL), design variants that adopt linear structural response (L) are considered; when performance objectives correspond risk-based quantification (R), design variants that adopt average performance quantification (A) are considered; when performance objectives correspond to non-stationary description using recorder ground motions (NS_r), design variants that adopt non-stationary description using stochastic ground motion modeling (NS) are considered.

The numerical results in Fig.6 confirm trends in Fig.5, showing that for VDs the modeling fidelity assumptions at the design stage have a small effect on the performance across various objectives. Note that for large dampers, represented by large values of J_2 objective (force demand), strong convergence is observed for the performance objectives of all design variants, across all fidelity assumptions considered. This is expected since for such larger dampers substantial vibration suppression is facilitated, as evident by the small J_1 values (building performance), reducing the importance of the details adopted for the device design. As such, differences observed around the middle of the Pareto front should be prioritized in evaluating the effectiveness of the different design variants. In this respect, the most significant differences occur for the designs that adopt a stationary excitation description while using recorded ground motions for performance assessment in Fig. 6(d). Further, in agreement with the correlation trends identified in Fig. 3, very good agreement is observed between the designs that adopt A performance quantification.

For the IVA implementation, substantially bigger differences exist for both structures, as evident from Figs. 7 and 8, with these differences being larger for structure B_2 (Fig. 7) for the reasons discussed previously, when examining trends in Fig. 5. Similar to the VD implementation, the simplified stationary assumption at the design stage leads always to largest discrepancies. Among the different design variants that use stationary assumption for the excitation, the one adopting the A performance quantification (the

Patsialis D, Taflanidis AA, Giaralis A (2023) Exploring the impact of excitation and structural response/performance modeling fidelity in the design of seismic protective devices. *Engineering Structures*, Accepted 13/2/2023.

popular \mathcal{H}_2 design) yields always very poor performance, while the design adopting the R performance quantification provides designs that are overall better aligned with higher fidelity objectives, exhibiting quite robust performance for some of the modeling cases considered. Explicit consideration of the nonlinearity of the response is important when combined with risk-based quantification of the performance [Figs. 7 and 8 (a) and (c)], and even creates discrepancies between the designs that utilize NS or NS_s excitation descriptions [Figs. 7 and 8 (c)] but adopt same assumptions for all other modeling aspects. On the other hand, for linear response, these design variants are more consistent with one another [Figs. 7 and 8 (b)]. The same applies for the average performance quantification even under nonlinear response [Figs. 7 and 8 (d)]. These trends indicate that the larger dispersion of the response for the NS_r excitation description impacts the quality of the design primarily only for the R performance quantification and nonlinear structural response.

Overall, the reduction of SPD efficiency observed in Figs. 6-8 for most of the simpler design variants (when compared against the actual Pareto fronts), clearly illustrates the potential pitfalls of using such simplified design approaches. Use of linear behavior assumptions, average performance quantification, or stationary excitation description can lead (in some cases) to substantially suboptimal designs. Especially for IVAs, the actual optimal device efficiency can be guaranteed only if the higher fidelity assumption is utilized. This also showcases the importance of computational advances, like the ROM formulation adopted in this study, that can accommodate the use of higher fidelity modeling assumptions for SPD design, alleviating some of the associated computational burden.

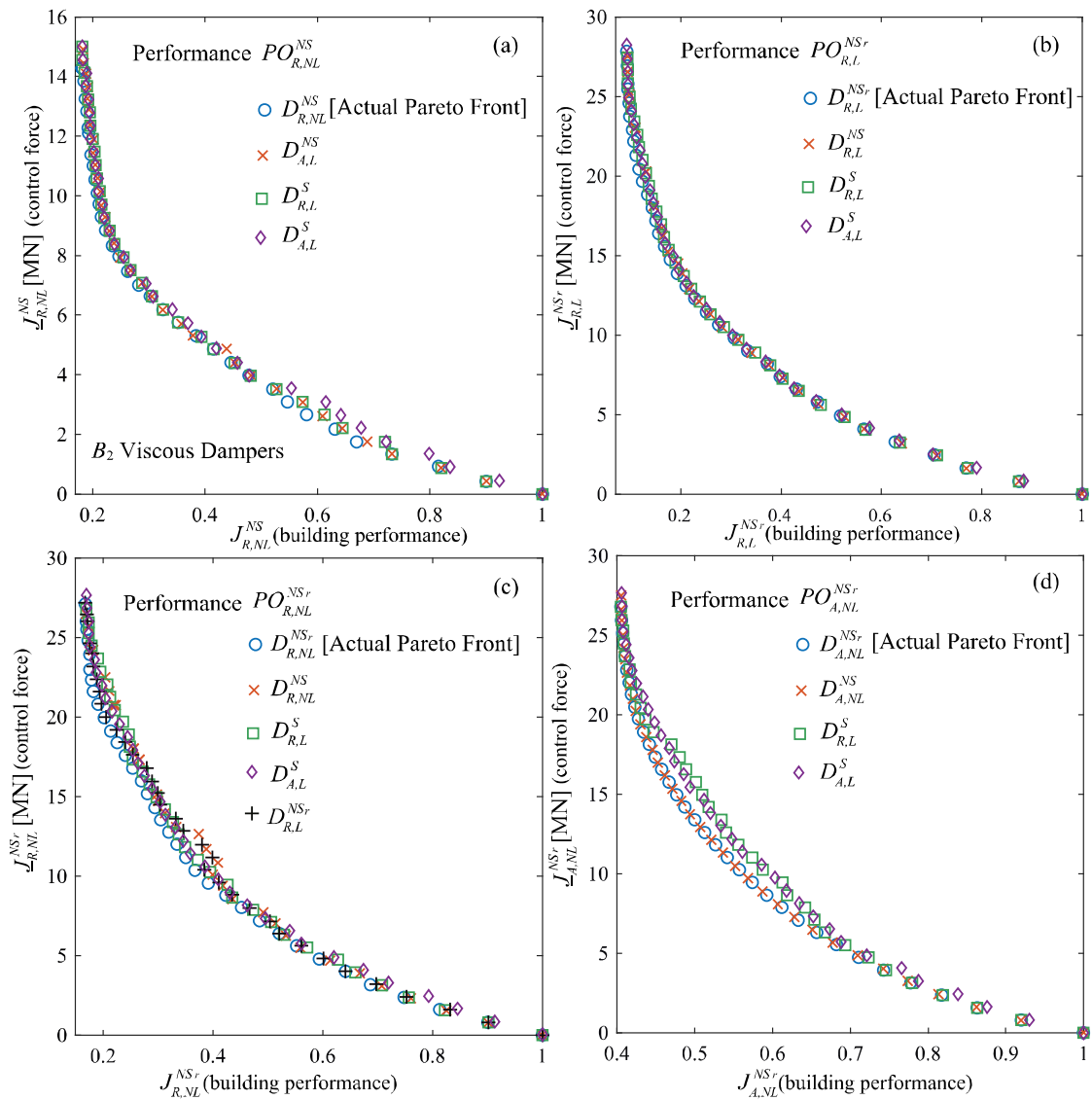


Fig. 6: Different performance objectives (subplots) for structure B_2 and VD implementation for balanced (O_3) consequence quantification. Linear and nonlinear response using NS and NS_r excitation description and for both risk or average performance quantification are considered. In each subplot the actual Pareto front is compared against the performance objectives achieved by different, simpler design variants.

Further additional interesting remarks can be drawn for the relative effectiveness of the SPDs for the different modeling settings by examining the normalized (by the performance of the uncontrolled building) J_1 values (building performance) achieved in each instance. Risk-based performance objectives appear to be reduced more substantially compared to average performance objectives, due to the ability of SPDs to suppress larger vibration responses and the greater contribution of these responses to the seismic consequences based on the Table 2 definitions. For the risk-based performance quantification, consideration

of nonlinear response yields a reduction of the SPD effectiveness, especially for the IVA implementations. This should be primarily attributed to the challenges of the single device to effectively control nonlinear responses across multiple floors, but also to the bigger effects of proper device tuning to the dynamic characteristics of the yielding structure. Similarly, reduction of effectiveness is observed for the NS_r excitation description. This is related to the way the largest response dispersion for this excitation description impacts the overall risk-based performance quantification.

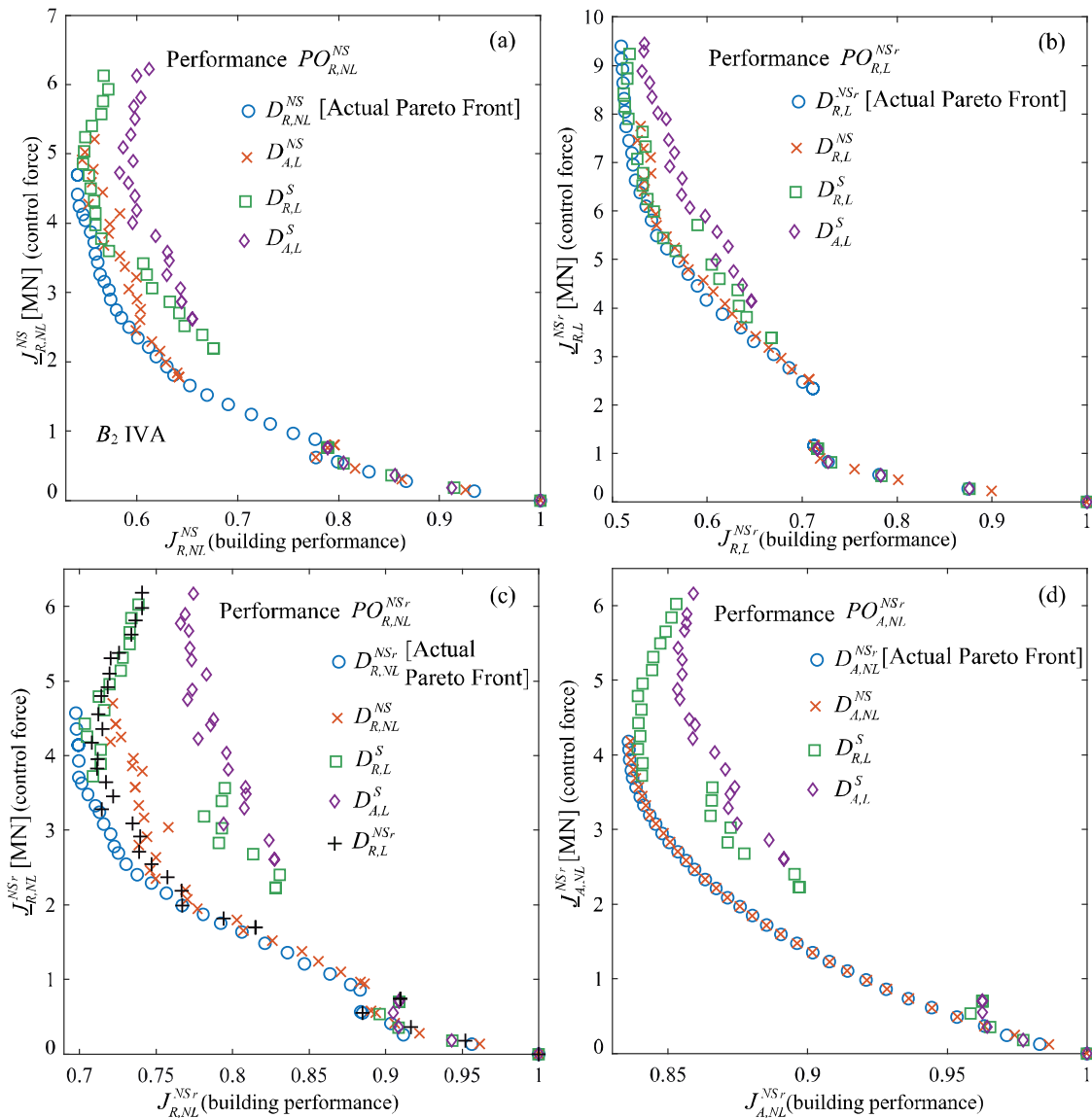


Fig. 7: Different performance objectives (subplots) for structure B_2 and IVA implementation for balanced (O_3) consequence quantification. Linear and nonlinear response using NS and NS_r excitation description and for both risk or average performance quantification are considered. In each subplot the actual Pareto front is compared against the performance objectives achieved by different, simpler design variants.

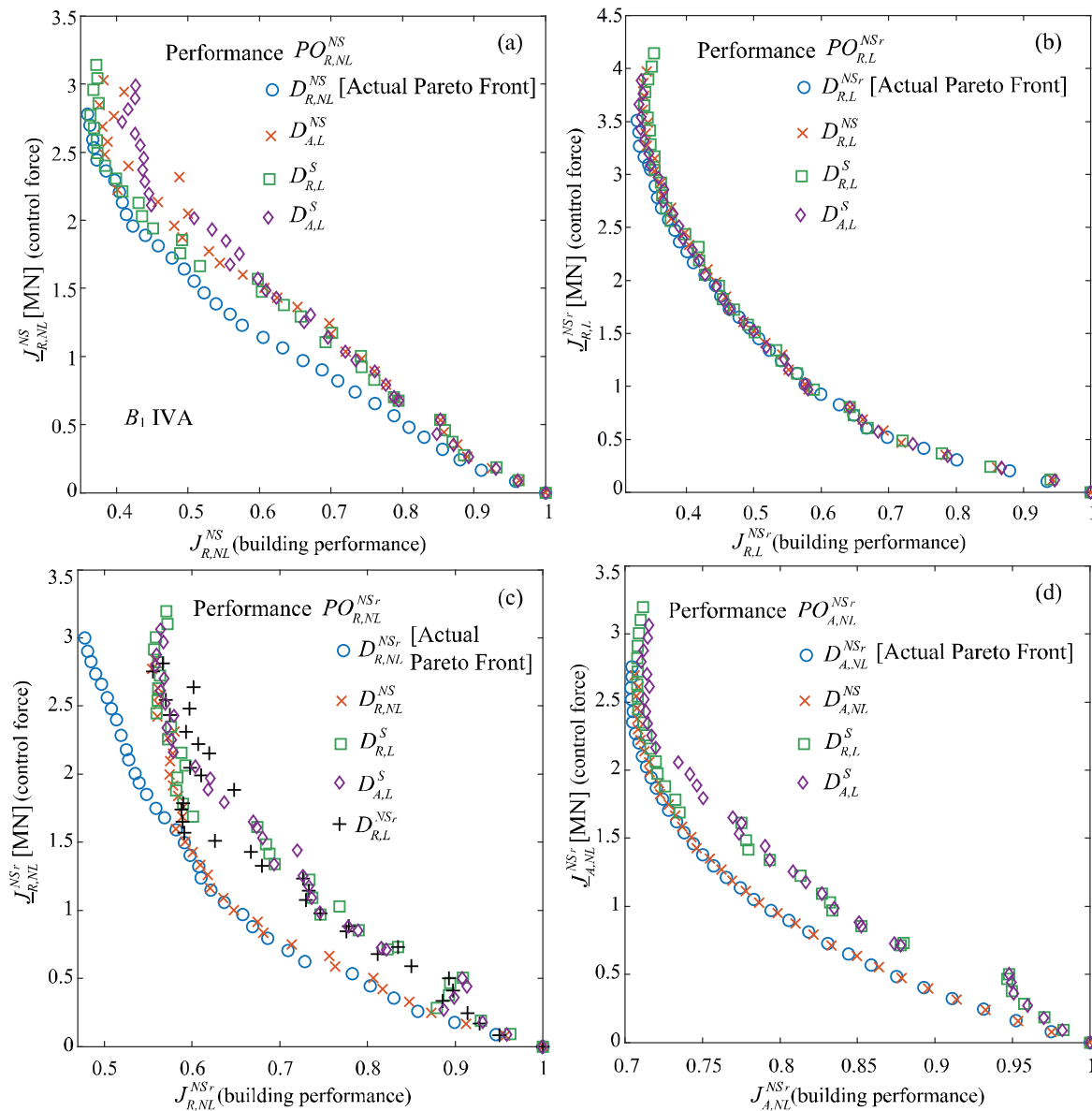


Fig. 8: Different performance objectives (subplots) for structure B_1 and IVA implementation for balanced (O_3) consequence quantification. Linear and nonlinear response using NS and NS_r excitation description and for both risk or average performance quantification are considered. In each subplot the actual Pareto front is compared against the performance objectives achieved by different, simpler design variants.

7.3 Comparison of performance for different types of IVAs

To shed light on the trends observed in previous figures for the IVA implementations, separate Pareto fronts for each of the three IVA types (TMD, TMDI and TID) are provided in Fig. 9. Though the trends are similar for other modeling assumptions, the main comparisons are established for the risk-based performance for two different design variants: nonlinear response and NS_r excitation description,

Patsialis D, Taflanidis AA, Giaralis A (2023) Exploring the impact of excitation and structural response/performance modeling fidelity in the design of seismic protective devices. *Engineering Structures*, Accepted 13/2/2023.

representing the design with higher fidelity modeling assumptions, and linear response and stationary excitation description, representing the design with lower fidelity modeling assumption. The top row [Fig. 9 (a) and (b)] of this figure presents the Pareto fronts for each of these design variants, separately for each IVA type. Note that the overall (actual) Pareto fronts for the corresponding IVA implementation reported in Figs. 5 and 7 earlier, are obtained by the leftmost members across the three IVA types, representing the group of dominant designs. It is evident from Fig.9 (a) and (b) that TMDI and TID establish very similar performance, especially for linear structural response, while fundamental different behavior is exhibited by the TMD. The latter device outperforms the TMDI and TID for small magnitude forces but cannot achieve similar degrees of vibration suppression, as it cannot achieve higher control forces (constraint by practical limitation to the TMD mass), as mentioned also earlier. The latter difference leads to a smaller range for the TMD Pareto front (compared to the other devices) and to a jump in the overall Pareto front when the dominance of the devices (TMD vs TID/TMDI) alters, while any transitions between TID and TMDI are smooth.

The more interesting comparisons is, though, in Fig. 9(c), which shows the performance objectives of the simplified designs when evaluated for the higher fidelity modeling assumptions. The performance objectives are shown separately for each of the three IVA devices, with the designs belonging to the IVA Pareto front for the simplified design (dominant designs across the three IVA devices) also shown. Results in this subplot should be compared to the actual Pareto front for this performance quantification, which is the one depicted in Fig. 9(a). Comparisons show that the TID provides a more robust behavior than the TMDI. For the latter, the addition of the secondary mass and the challenges that are associated with activating this secondary mass for vibration suppression for non-stationary excitations [85, 86] evidently reduce its design robustness. Notably, even though when designed under correct assumptions the TMDI provides comparable efficiency to the TID [Fig. 9(a)], when stationary assumptions are utilized at the design stage, the corresponding efficiency under non-stationary excitation is reduced [Fig. 9(c)]. Furthermore, even though the performance objectives for each device exhibit consistent trends in Fig. 9(c), when the

designs representing the overall IVA implementation are considered [squared dots in Fig.9(c)], the aforementioned differences in the behavior create separate clusters. This pattern is evident across multiple other modeling variants, as also seen previously in Figs 5, 7 and 8.

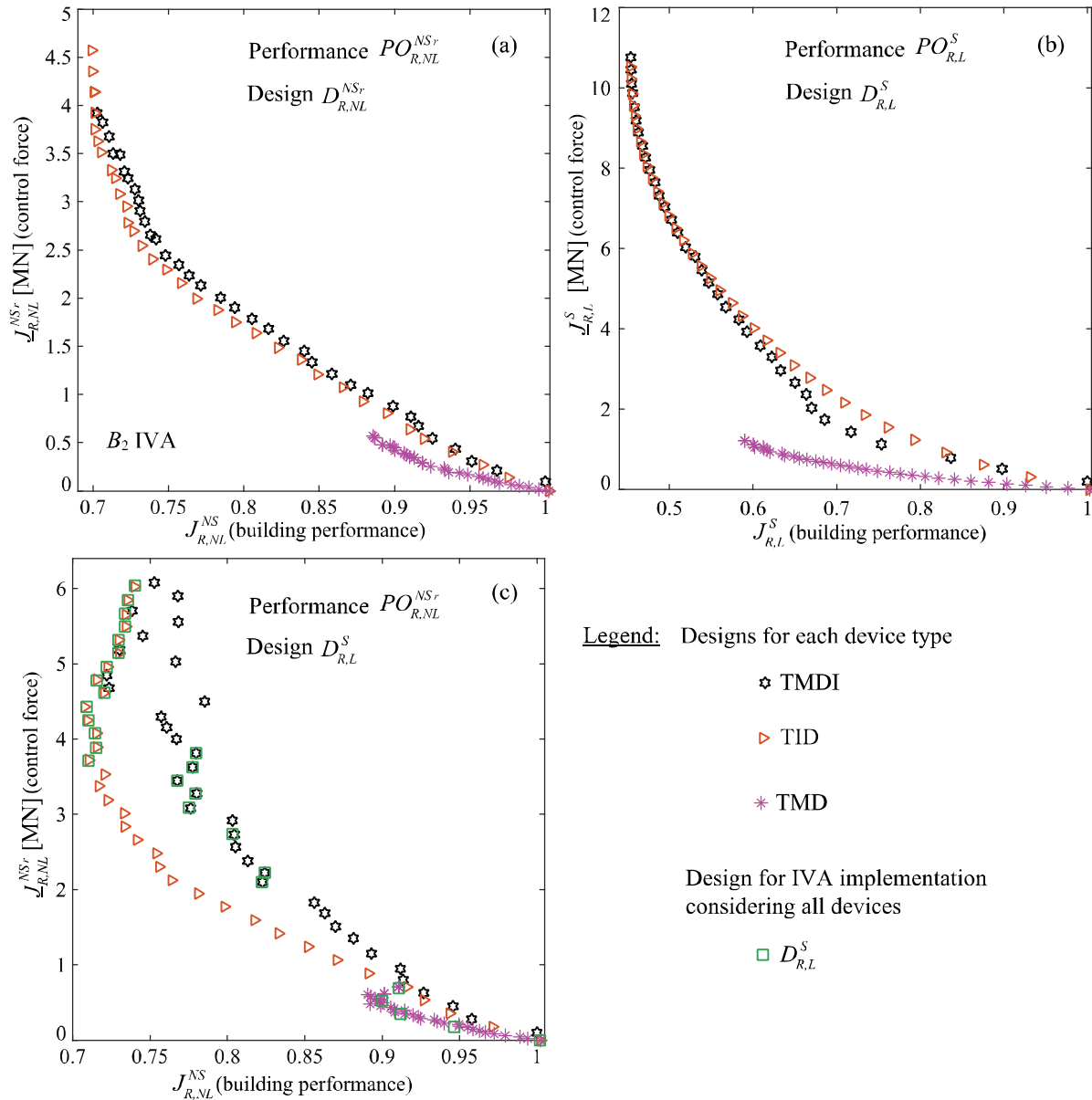


Fig. 9: Performance for structure B_2 for each of the three different type of IVA devices (TMDI, TID, TMD) for risk-based performance and balanced (O_3) consequence quantification for two different designs variants: nonlinear response and NS_r excitation description (higher fidelity assumption) and linear response and stationary excitation description (simplified assumption). Top row shows Pareto fronts for each of the designs, while bottom row reports the performance objectives of the simplified design when evaluated for the higher fidelity modeling assumptions.

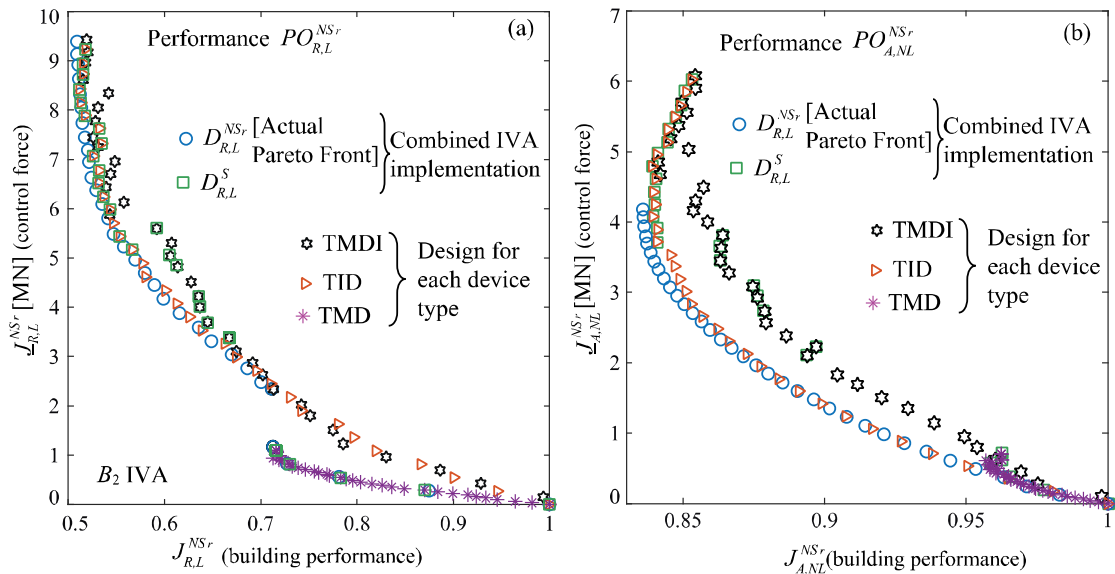


Fig. 10: Performance objectives for structure B_2 for each of the three different type of IVA devices (TMDI, TID, TMD) for linear risk-based and nonlinear average performance and for balanced (O_3) consequence quantification for two different designs variants: the corresponding Pareto front (higher fidelity assumption) and linear response and stationary excitation description (simplified assumption).

To further showcase these trends, Fig. 10 replicates Fig. 9 (c) for two other performance objectives, for linear response and risk-based performance quantification [Fig. 10(a)] and nonlinear response and average performance quantification [Fig. 10(b)]. In both instances recorded ground motions are used for the excitation description (NS_r). Performance for the respective objective of the risk-based stationary design variant is plotted for each of the three different type of IVA devices along with the actual Pareto front. Trends are identical to Fig. 9 (c), demonstrating that: (i) the behavior identified previously in Figs. 5, 7 and 9 can be attributed to differences between the different devices that are combined under the IVA implementation umbrella; and (ii) the TID implementation enjoys greater design robustness.

7.4 Influence of number of ground motions in SPD design variants using recorder ground motions

For the SPD designs that utilize recorded ground motions for the excitation description (NS_r) the number of ground motions used can have an important influence on the design. This influence is investigated in Figs. 11 and 12 by comparing the Pareto front derived using the larger number of ground motions, against the performance objectives achieved by designs established using a small number of only

7 ground motions. For each plot in these figures, three such simplified designs are presented, corresponding to different ground motion selection. Fig. 11 presents results for structure B_2 and VDs and Fig. 12 results for structure B_2 and IVAs. Trends for structure B_1 are identical. The comparisons are established for both linear and nonlinear response and for both risk and average performance quantification.

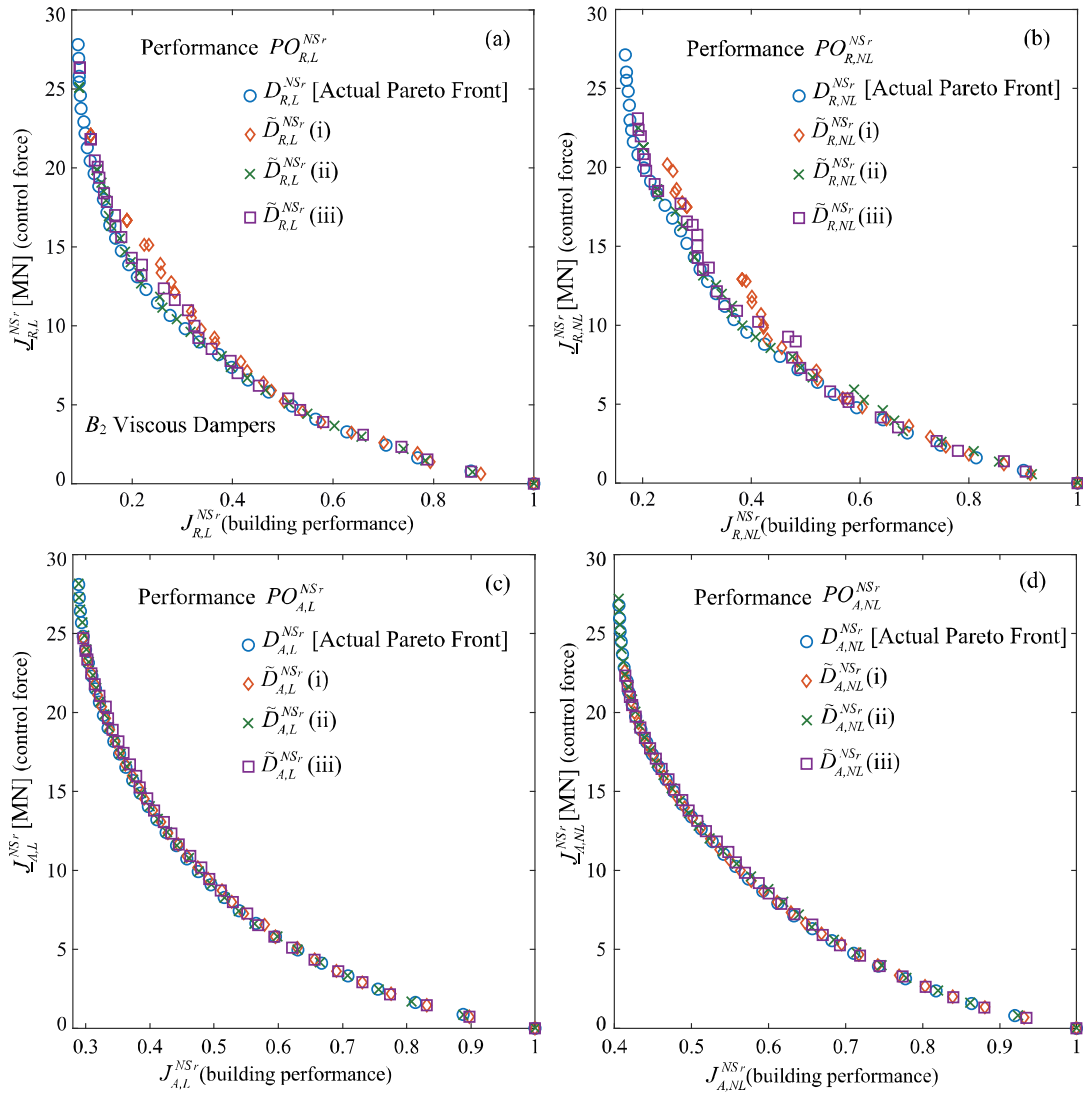


Fig. 11: Impact on the design of the number of ground motions considered for the NS_r excitation description for structure B_2 and VD devices, for the balanced (O_3) consequence quantification. Objectives for both linear and nonlinear response and for both risk and average performance quantification is shown. The Pareto front established by considering large number of ground motions is compared against the performance objectives achieved by three simplified designs that consider a small number of 7 ground motions (different ground motion for each).

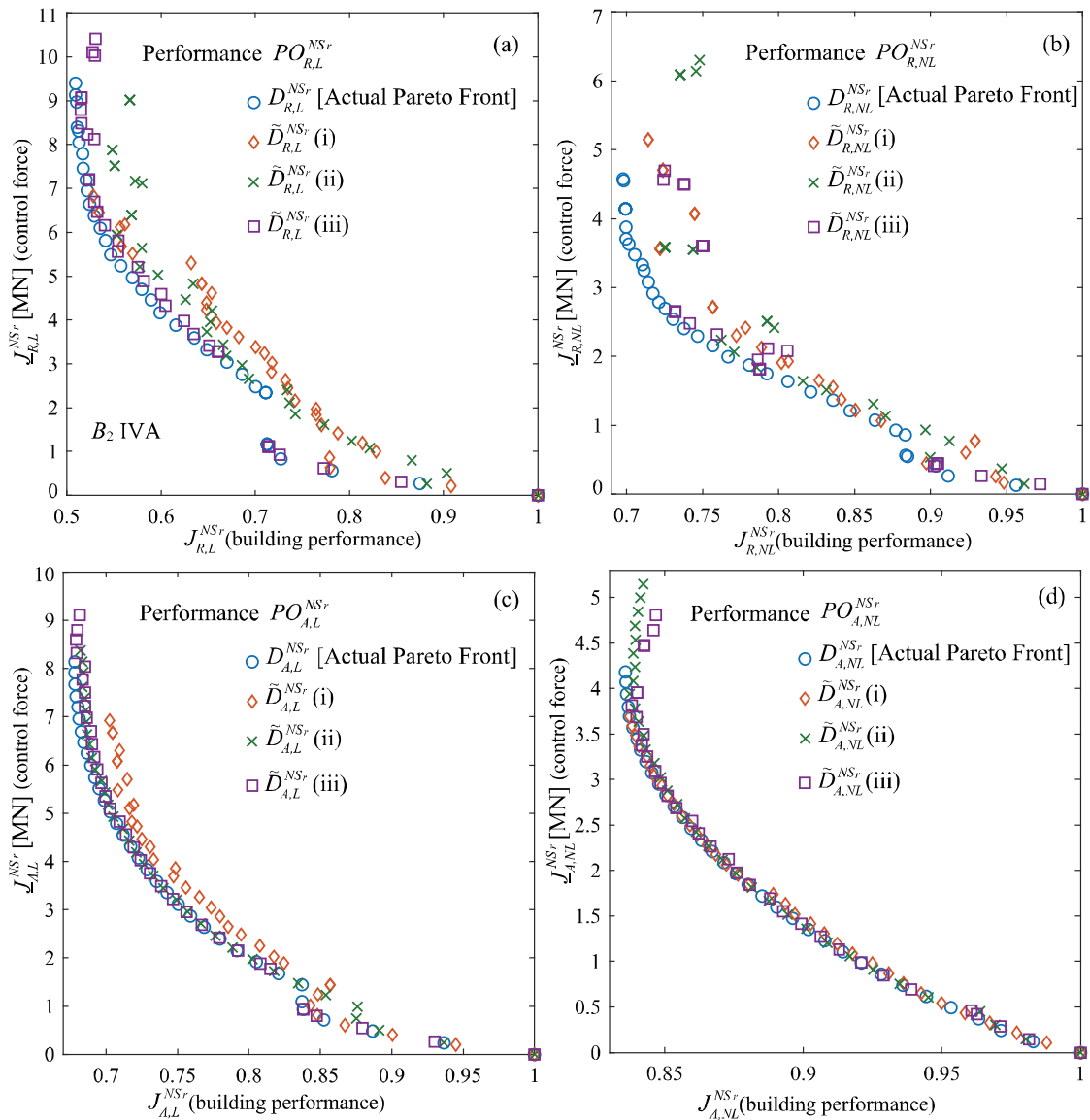


Fig. 12: Impact on the design of the number of ground motions considered for the NS_r excitation description for structure B_2 and IVA devices, for the balanced (O_3) consequence quantification. Objectives for both linear and nonlinear response and for both risk and average performance quantification is shown. The Pareto front established by considering large number of ground motions is compared against the performance objectives achieved by three simplified designs that consider a small number of 7 ground motions (different ground motion for each).

Results indicate that for VDs the influence of the selected ground motions is considerable for the R performance quantification [Fig.11(a) and (b)], especially for nonlinear response, and small for the A performance quantification. Same general trends hold for the IVAs (Fig. 12), through the general differences in this case are significantly higher. The differences in the trends between the different devices are impacted partly by their respective dynamic characteristics and interactions with the building structure,

Patsialis D, Taflanidis AA, Giaralis A (2023) Exploring the impact of excitation and structural response/performance modeling fidelity in the design of seismic protective devices. *Engineering Structures*, Accepted 13/2/2023.

which is more critical for inertia-based vibration absorbers (IVAs), and partly by the different degree of vibration suppression each SPD can offer, which is higher for VDs for the reasons discussed in section 7.2. Overall, the comparisons illustrate that the use of small number of ground motions at the design stage, even though computationally efficient, may yield suboptimal designs solution when examined for realistic assumptions: nonlinear response and risk-based performance quantification.

7.5 Influence of the consequence quantification on the design variant comparisons

In all previous results presented, the balanced consequence quantifications has been considered. This last section presents representative results for the two other consequence quantifications, the drift sensitive (O_1) and acceleration sensitive (O_2). Fig. 13 shows results for the VD implementation for structure B_2 , Fig. 14 for the IVA implementation for structure B_2 and Fig. 15 for the IVA implementation for structure B_1 . VD implementation for structure B_1 has similar trends with the one of B_2 and is omitted here due to space limitation. In each figure, different performance variants (subplots) are examined for drift-sensitive (O_1) [left column] and acceleration-sensitive (O_2) [right column] consequence quantifications. In all instances, the NS_r excitation description is adopted, representing the most realistic model for future excitations, while for the other modeling assumptions, both linear and nonlinear structural response and both risk-based or average performance quantification are examined. As in previous results, the actual Pareto front for each case is compared against the performance objectives achieved by different, simpler design variants.

Results for VD (Fig. 13) show greater impact of the design assumptions for drift-sensitive consequence quantification, with most alternative design variants exhibiting greater departure from the actual Pareto front. For the acceleration-sensitive or balanced consequence quantification such departures are primarily observed for design variants that adopt very simplistic assumptions: stationary excitation description and average performance quantification. For drift-sensitive design, even greater departure from the optimal performance is observed for the aforementioned simplistic designs, but, additionally, differences are observed for other design variants with modeling assumptions that are more compatible to the performance objectives examined. For example, for the risk-based performance quantification [Fig. 13(a)] the non-

stationary excitation description (NS instead of NS_r) as well as the structural response (L instead of NL) have important effects on the achievable device performance.

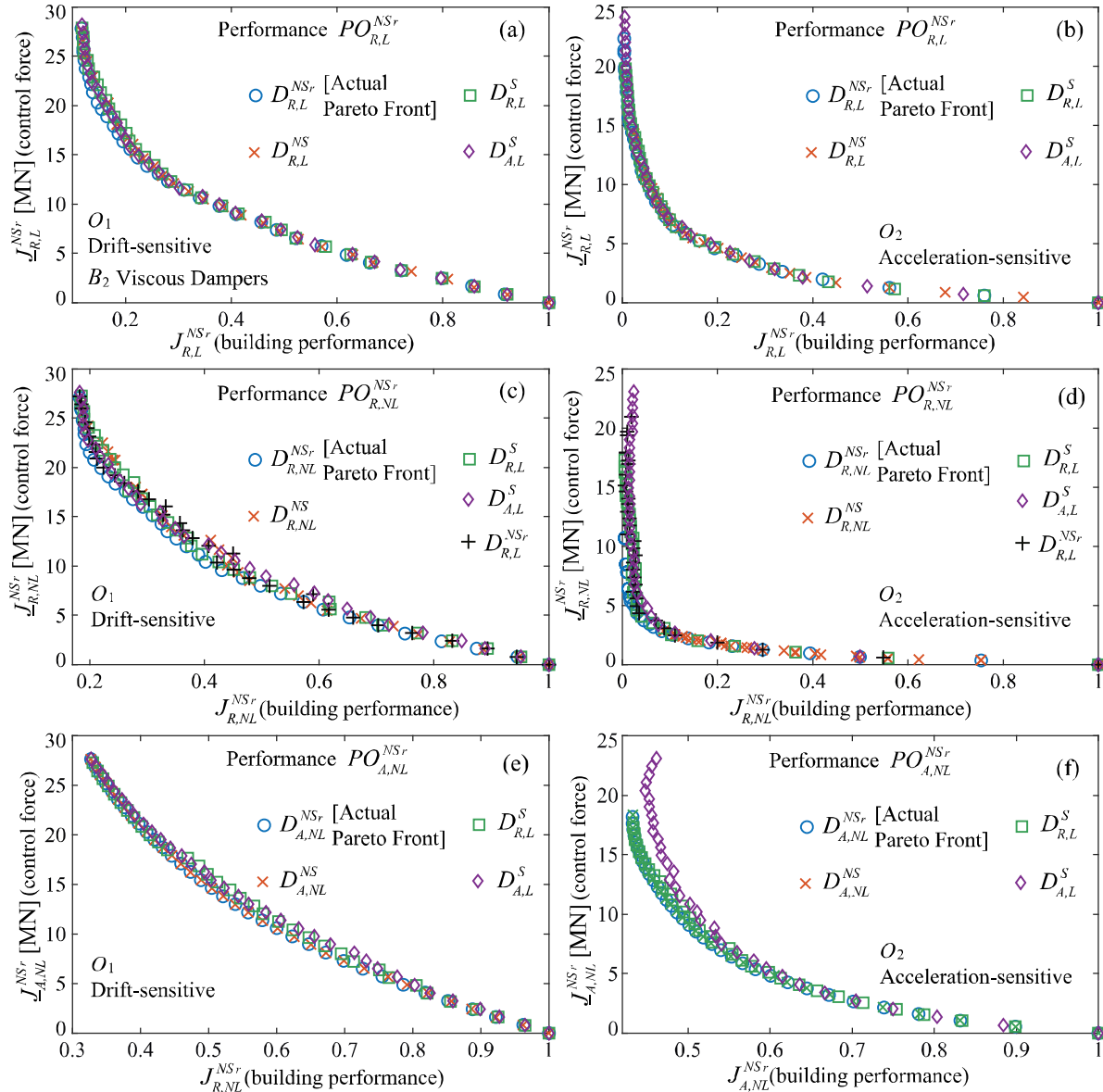


Fig. 13: Different performance objectives (subplots) for structure B_2 and VD implementation for drift-sensitive (O_1) [left column] and acceleration-sensitive (O_2) [right column] consequence quantifications. Linear and nonlinear response using NS_r excitation description and for both risk or average performance quantification are considered. In each subplot the actual Pareto front is compared against the performance objectives achieved by different, simpler design variants.

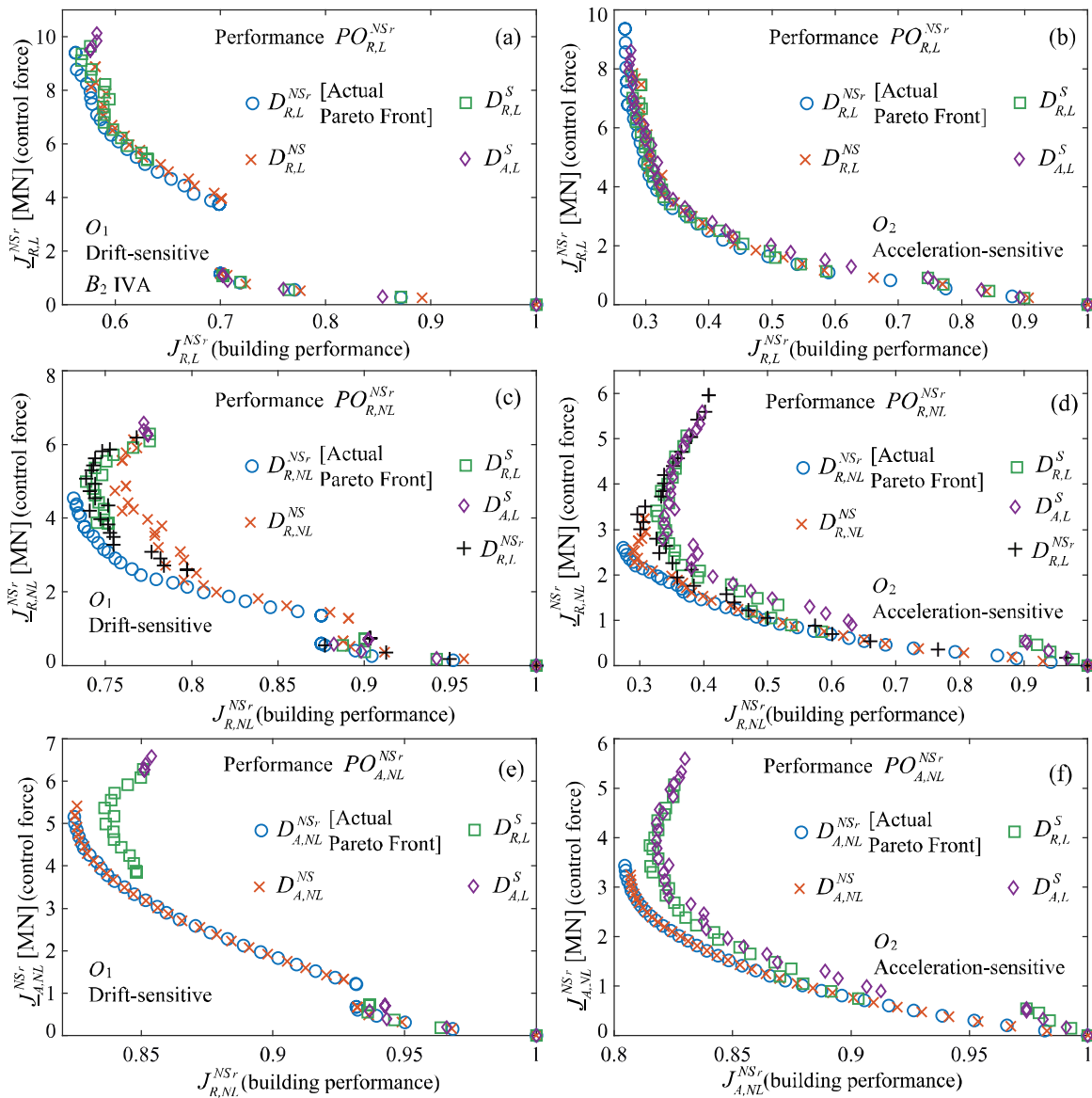


Fig. 14: Different performance objectives (subplots) for structure B_2 and IVA implementation for drift-sensitive (O_1) [left column] and acceleration-sensitive (O_2) [right column] consequence quantifications. Linear and nonlinear response using NS_r excitation description and for both risk or average performance quantification are considered. In each subplot the actual Pareto front is compared against the performance objectives achieved by different, simpler design variants.

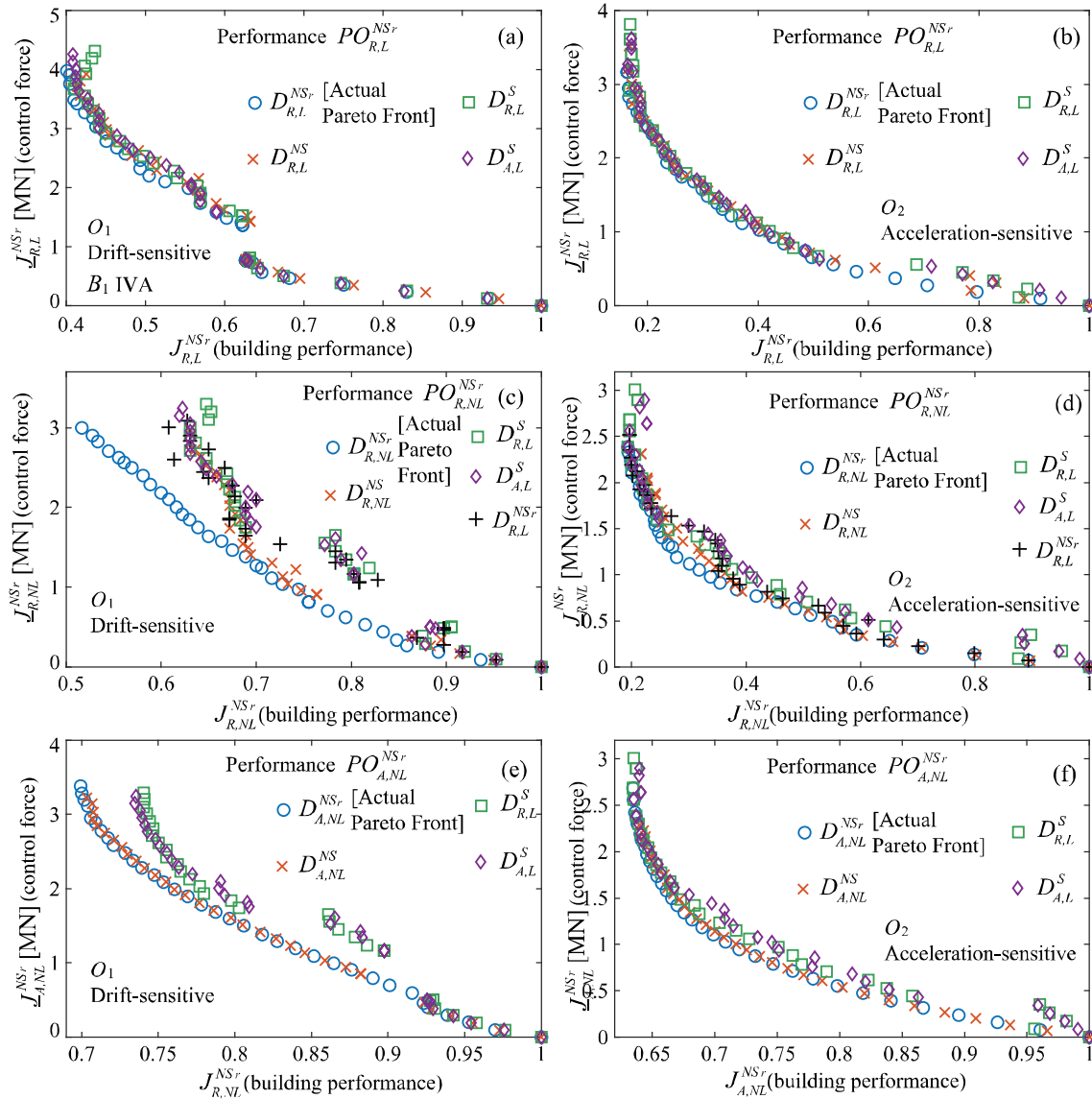


Fig. 15: Different performance objectives (subplots) for structure B_1 and IVA implementation for drift-sensitive (O_1) [left column] and acceleration-sensitive (O_2) [right column] consequence quantifications. Linear and nonlinear response using NS_r excitation description and for both risk or average performance quantification are considered. In each subplot the actual Pareto front is compared against the performance objectives achieved by different, simpler design variants.

Focusing next on the IVA implementation (Figs. 14 and 15), it is evident that larger differences are observed in the trends across the different ranges of the performance objectives for drifts and acceleration sensitive designs. Specifically, the design variants corresponding to stationary modeling assumptions populate only the extreme parts of the performance objectives for drift-sensitive design, while there is no

Patsialis D, Taflanidis AA, Giaralis A (2023) Exploring the impact of excitation and structural response/performance modeling fidelity in the design of seismic protective devices. *Engineering Structures*, Accepted 13/2/2023.

jump between TMDI/TID and TMD implementations for the Pareto front for the acceleration-sensitive designs. This behavior is attributed to the unique behavioral characteristics of the TMD implementation, as also showcased in past studies that have established comparisons between TMDIs and TMD devices [9, 24, 38] or have examined in detail the seismic performance of TMDs [85, 86]. In particular, the tuning of TMDs to a specific mode reduces their ability to suppress acceleration responses for taller structures with important higher frequency dynamics like structure B_2 in Fig. 14 (greater relative impact of such dynamics on acceleration responses), as well as their ability to offer protection when building is experiencing nonlinear behavior that alters its modal properties. Further, the TMD inertia-based principle of operation reduces their protection efficiency for non-stationary excitations (compared to their efficiency for stationary excitations) due to the slower activation of the device at earlier parts of the ground motion excitation. For these reasons, TMDs might not merge as dominant designs over TMDI/TID implementations (and not appear in the Pareto front) for acceleration-sensitive consequence quantifications, especially when considering nonlinear behavior and/or non-stationary excitation description (combination of multiple sources of efficiency reduction) as shown in parts (b), (d) and (f) in Figs.14 and 15. Moreover, the dominance of the TMDs under stationary excitation for drift-sensitive consequences is not translated to other performance quantifications, creating significant differences in the performance of design solutions corresponding to TMD or TMDI/TID implementations, when such solutions are obtained using stationary assumptions as shown in parts (a), (c) and (e) in Figs.14 and 15. These discussions clearly showcase the importance of the modeling fidelity in designing TMDs and in comparing their seismic protection efficiency to inerter-based devices.

Extending the comparisons in Figs. 14 and 15 across the complete IVA implementation, similar trends hold for all consequence quantifications, with alternative design variants losing efficiency when compared against the actual Pareto front. Nevertheless, the degree of this reduction, and the corresponding loss of robustness of the simplified design approaches depends on the specifics of the consequence quantification. When combined with the trends observed for the VD implementation (Fig. 13), this further stresses that the degree of compatibility of the design variants is dependent on the consequence quantification details (i.e.

Patsialis D, Taflanidis AA, Giaralis A (2023) Exploring the impact of excitation and structural response/performance modeling fidelity in the design of seismic protective devices. *Engineering Structures*, Accepted 13/2/2023.

choice of EDPs and their relative weight in the SPD design), on top of the level of modelling fidelity discussed in previous sections (i.e. risk-based instead of average performance). For certain consequence quantifications bigger discrepancies may exist between the design variants. As a final remark, it is important to note that this dependency on EDPs is case-sensitive as it is influenced not only by the building properties, but also by the consequence function details (see Table 2). The parametric investigation of the latter aspect falls outside the scope of this work.

8. Conclusions

The impact of modeling fidelity on the design of seismic protective devices (SPDs) was numerically examined in this paper, focusing on different aspects of the problem formulation: characterization of dynamic earthquake excitations, evaluation of the seismic structural response and quantification of the seismic performance. For each of the three considered modeling aspects, different fidelity models were selected to examine the required level of modelling sophistication in the SPD design that provides favorable outcomes when assessed using realistic modeling assumptions. For the excitation, both stationary and non-stationary descriptions were adopted, while for the non-stationary formulation the use of either stochastic ground motion models or scaling of recorded ground motions was considered using different numbers of records. For the structural response, the use of either linear or non-linear structural models was examined, and for the performance quantification, both average response and risk-based estimation was considered, using different EDPs (minimizing storey drifts, or floor accelerations, or both). Combination of models across the three different modeling aspects established a large model hierarchy and resulted in multiple SPD design variants obtained using a bi-objective framework that considers the competing structural vibration suppression (building performance) and device control forces as distinct objectives.

The illustrative implementation considered a 3-storey and a 9-storey steel benchmark buildings, equipped with two different classes of SPDs: viscous dampers (VDs) and inertial vibration absorbers (IVAs), including the tuned-inerter-damper (TID), the tuned-mass-damper-inerter (TMDIs) and the tuned-mass-damper (TMD). For these structures and SPDs, some comparisons were established across pairs of

Patsialis D, Taflanidis AA, Giaralis A (2023) Exploring the impact of excitation and structural response/performance modeling fidelity in the design of seismic protective devices. *Engineering Structures*, Accepted 13/2/2023.

related performance objectives within the established model fidelity hierarchy, though the detailed investigation of the impact of model fidelity was established by comparing the performance objectives achieved by optimal designs using different fidelity assumptions. In all instances, the actual Pareto front was compared to the performance objectives achieved by simplified design variants. This innovative methodological approach enabled comprehensive comparisons across the model hierarchy. The resulting major overarching concluding remarks are as follows:

- Single IVA device implementations were found to be more sensitive to the fidelity of design modelling assumptions than distributed VDs across all building floors. In particular, for large control force VDs, performance is practically identical across all the different VD design fidelity models for both the considered benchmark structures. In this regard, the use of several large VDs (one in each floor) achieves significant gains in terms of design robustness at the expense of expectedly higher device costs and structural/architectural interventions to accommodate the devices, compared to single IVA device installations (in one floor only).
- Focusing on the differences across the examined IVAs, it was established that the TID is more robust to the fidelity of the design modelling assumptions compared to the TMDI. Even though the TMDI provides comparable efficiency to the TID when assessed with the same assumptions used in the tuning stage, when stationary excitation assumption is adopted for the TMDI tuning, the corresponding efficiency under non-stationary excitations is significantly reduced compared to the TID. Therefore, adopting more lightweight IVAs (i.e. where most/all of the inertia comes from the inertance property rather than from the secondary mass) relaxes requirements for high-fidelity device tuning.
- The seismic performance of the taller 9-storey benchmark building was found to be consistently more sensitive to the fidelity of SPD design modelling compared to the 3-storey benchmark building. This is readily attributed to the fact that suppressing higher mode contributions becomes more challenging, especially for single IVA device implementations and for floor acceleration EDPs, thus SPD design details become more critical. Consequently, the effective treatment of taller structures requires higher

fidelity SPD design assumptions, resulting in significant higher computational costs for structures that, by default, will involve larger and/or more complex computational models.

- For intermediate building performance (i.e. close to the middle of the Pareto front), the (low-fidelity) stationary excitation assumption vis-à-vis the (high-fidelity) non-stationary excitation leads consistently to the highest performance discrepancies (i.e. higher control force) compared to all other design modelling assumptions examined for all SPDs and for both buildings considered. This is especially true for risk-based performance metrics. Thus, an important conclusion of the study is that in this range of building performance, adopting stationary excitation for SPD design leads to unnecessary conservative designs or, equivalently, to reduced SPD efficiency.
- For high building performance (i.e. close to the extreme of the Pareto front corresponding to a minimum for the building vibration), significant deviations from Pareto optimal performance were found when adopting uniformly modulated in time artificial non-stationary ground motions as opposed to recorded ground motions for IVA optimal tuning using risk-based metrics. Deviations were appreciably more significant for the more challenging case of protecting the 9-storey building. It is thus recommended for the risk-based IVA design to adopt as a realistic (high-fidelity) as possible seismic excitation model when aiming to achieve high-performing high-rise buildings, which further highlights the importance of using state-of-art computational tools to treat such demanding applications.
- Consideration of structural nonlinear response becomes important in the SPD design when combined with risk-based performance quantification as opposed to average performance. Moreover, the risk-based performance of nonlinear structures becomes sensitive to the use of recorded ground motions as opposed to artificial ground motions with only time-domain non-stationarity, as well as to the number of recorded ground motions used. It is thus concluded that balance of the level of fidelity across the three examined SPD design aspects is critical, in alignment with modern PBEE practices.

- Under the low-fidelity SPD design assumptions of linear structural response and/or average performance metrics (i.e. the popular H_2 design), design variants were found to be consistent across structures and types of SPDs. Nevertheless, since response of actual structures under severe ground shaking is likely to be nonlinear while performance and seismic consequences are more realistically described utilizing a risk-based quantification, the reduction of SPD efficiency observed for the simpler design variants (when compared against the actual Pareto fronts), clearly illustrates a reduction in vibration protection when using simplified low-fidelity SPD design approaches. Especially for IVAs, the actual optimal device efficiency can be guaranteed only for higher fidelity design assumptions. Once again, the need for modern structural dynamics computational tools which can reduce computational costs without compromising accuracy is emphatically highlighted.

Overall, the comparisons demonstrate the potential pitfalls of using simplified modeling assumptions at the design stage and showcases the importance of computational advances, like the ROM formulation adopted in this study, that can accommodate the use of higher fidelity modeling assumptions for SPD design, alleviating the associated computational burden. They also showcased the benefits accommodated through the examination of the modeling fidelity across all three aspects of the SPD design problem formulation, emphasizing both individual descriptors as well as the hierarchy of models obtained through their combination: through the hierarchical comparisons key insights were identified for the behavior of the different type of SPD devices and for the robustness characteristics of the different design approaches. Though such insights can be related to fundamentals of the dynamic behavior of each device, their identification through comparisons of the device efficiency across the different design variants is a significant benefit of the herein obtained hierarchical comparisons, and stresses the importance for establishing such type of comparisons in gaining better understanding of the strengths and vulnerabilities of SPDs. Finally, it is important to acknowledge that the large scale of the study, exploring fidelity across three diverse aspects of the problem formulation, inevitably enforced some restrictions in its scope and breadth of the different fidelity assumptions that could be explored. Perhaps the most important relevant

limitation is on the aspects of nonlinear behavior incorporated in this study, since nonlinearities relevant to the SPDs themselves were not considered at all (and these can be important), whereas for the structural only hysteretic structural behavior was addressed.

Appendix A. Details for the state-space formulation

The stationary excitation model with power spectral density $S_g(\omega)$ can be described through state space model:

$$\begin{aligned}\dot{\mathbf{x}}_q(t) &= \mathbf{A}_q \mathbf{x}_q(t) + \mathbf{E}_q w(t) \\ \ddot{\mathbf{x}}_g(t) &= \mathbf{C}_q \mathbf{x}_q(t),\end{aligned}\tag{A.1}$$

where $w(t) \in \mathfrak{R}$ is a zero-mean Gaussian white-noise process with spectral intensity equal to $S_w=1/(2\pi)$, $\mathbf{x}_q(t) \in \mathfrak{R}^{n_q}$ is the state vector for the excitation, $\mathbf{A}_q \in \mathfrak{R}^{n_q \times n_q}$, $\mathbf{E}_q \in \mathfrak{R}^{n_q \times 1}$ and $\mathbf{C}_q \in \mathfrak{R}^{1 \times n_q}$ are the state-space excitation matrices, chosen so that state-space model of Eq. (A.1) leads to output $\ddot{\mathbf{x}}_g(t)$ having spectral description $S_g(\omega)$. It should be noted that such a finite dimensional state-space representation can be accommodated only if $S_g(\omega)$ corresponds to a rational function. This is true for the high-pass Kanai-Tajimi spectrum of Eq. (1), for which the definition of the relevant matrices is:

$$\begin{aligned}\mathbf{A}_q &= \begin{bmatrix} 0 & 1 & 0 & 0 \\ -\omega_g^2 & -2\zeta_g \omega_g & 0 & 0 \\ 0 & 0 & 0 & 1 \\ -\omega_g^2 & -2\zeta_g \omega_g & -\omega_f^2 & -2\zeta_f \omega_f \end{bmatrix} & \mathbf{E}_q &= \begin{bmatrix} 0 \\ 1 \\ 0 \\ 0 \end{bmatrix} \\ \mathbf{C}_q &= \sigma_o \begin{bmatrix} -\omega_g^2 & -2\zeta_g \omega_g & \omega_f^2 & 2\zeta_f \omega_f \end{bmatrix}\end{aligned}\tag{A.2}$$

where σ_o is chosen such that the excitation has the desired a_{RMS} intensity.

For the linear structure with viscous dampers, characterized by Eq. (6) with the substitution of linear restoring forces as discussed in section 3.2, the equivalent state-space description is

$$\begin{aligned}\dot{\mathbf{x}}_t(t) &= \mathbf{A}_s(\boldsymbol{\varphi}) \mathbf{x}_t(t) + \mathbf{E}_s(\boldsymbol{\varphi}) \ddot{\mathbf{x}}_g(t) \\ \mathbf{z}(t) &= \mathbf{C}_s(\boldsymbol{\varphi}) \mathbf{x}_t(t),\end{aligned}\tag{A.3}$$

where $\mathbf{x}_t \in \mathfrak{R}^{n_t}$ (with $n_t=2n$ in this case) is the state vector collecting relative to the ground displacements and velocities of all stories $\mathbf{x}_t = [\mathbf{x}_s^T \quad \dot{\mathbf{x}}_s^T]^T$, $\mathbf{z} \in \mathfrak{R}^{n_z}$ is the desired output variables (as needed to define the desired performance quantities), dependencies on the design vector $\boldsymbol{\varphi}$ as defined in Section 4.1 is explicitly denoted, and the matrices in Eq. (A.3) are:

$$\begin{aligned} \mathbf{A}_s(\boldsymbol{\varphi}) &= \begin{bmatrix} \mathbf{0}_{n \times n} & \mathbf{I}_n \\ -\mathbf{M}_s^{-1} \mathbf{K}_s & -\mathbf{M}_t^{-1} (\mathbf{C}_s + \mathbf{R}_v^T \text{diag}(\mathbf{c}_v) \mathbf{R}_v) \end{bmatrix} \\ \mathbf{E}_s(\boldsymbol{\varphi}) &= \begin{bmatrix} \mathbf{0}_{n \times 1} \\ -\mathbf{R}_s \end{bmatrix}; \quad \mathbf{C}_s(\boldsymbol{\varphi}) = \begin{bmatrix} \text{diag}(1/\mathbf{h}) \mathbf{T}_s & \mathbf{0}_{n \times n} \\ [\mathbf{0}_{n \times n} & \mathbf{I}_n] \mathbf{A}_s(\boldsymbol{\varphi}) \\ \text{diag}(\mathbf{c}_v) \mathbf{R}_v [\mathbf{0}_{n \times n} & \mathbf{I}_n] \end{bmatrix} \end{aligned} \quad (\text{A.4})$$

The definition of the output matrix $\mathbf{C}_s(\boldsymbol{\varphi})$ in this equation corresponds to output variable vector \mathbf{z} that includes inter-storey drift ratios and absolute accelerations for all floors, and damper forces. Further, \mathbf{I}_a is the identity matrix of dimension a , $\mathbf{0}_{a \times b}$ is the zero matrix of dimensions $a \times b$, and $\text{diag}(1/\mathbf{h})$ is a diagonal matrix with elements the reciprocals of the height of each story, used to convert inter-storey drifts to drift ratios.

For the linear structure with the IVA, characterized by Eq. (8) with the substitution of linear restoring forces as discussed in section 3.2, the equivalent state-space description takes the same form of Eq. (A.3) but in this case the state vector $\mathbf{x}_t \in \mathfrak{R}^{n_t}$ (with $n_t=2n+2$) includes the relative to the ground displacements and velocities of all stories and of the spring/inerter connection point relative to i_b floor, $\mathbf{x}_t = [\mathbf{x}_s^T \quad y \quad \dot{\mathbf{x}}_s^T \quad \dot{y}]^T$, while the state and output matrices are defined as:

$$\begin{aligned} \mathbf{A}_s(\boldsymbol{\varphi}) &= \begin{bmatrix} \mathbf{0}_{(n+1) \times (n+1)} & \mathbf{I}_{(n+1)} \\ -\mathbf{M}_t(\boldsymbol{\varphi})^{-1} \begin{bmatrix} \mathbf{K}_s & \mathbf{0}_{n \times 1} \\ \mathbf{0}_{1 \times n} & k_d \end{bmatrix} & -\mathbf{M}_t(\boldsymbol{\varphi})^{-1} \begin{bmatrix} \mathbf{C}_s & \mathbf{0}_{n \times 1} \\ \mathbf{0}_{1 \times n} & c_d \end{bmatrix} \end{bmatrix} \\ \mathbf{E}_s(\boldsymbol{\varphi}) &= \begin{bmatrix} \mathbf{0}_{(n+1) \times 1} \\ -\mathbf{M}_t(\boldsymbol{\varphi})^{-1} \begin{bmatrix} \mathbf{M}_s + \mathbf{R}_d m_d \mathbf{R}_d^T \\ m_d \mathbf{R}_d^T \end{bmatrix} \mathbf{R}_s \end{bmatrix}; \quad \mathbf{C}_s(\boldsymbol{\varphi}) = \begin{bmatrix} \text{diag}(1/\mathbf{h}) \mathbf{T}_s & \mathbf{0}_{m \times (n+2)} \\ [\mathbf{0}_{n \times (n+1)} & \mathbf{I}_n & \mathbf{0}_{n \times 1}] \mathbf{A}_s(\boldsymbol{\varphi}) \\ b [\mathbf{R}_c^T & \mathbf{1}] [\mathbf{0}_{(n+1) \times (n+1)} & \mathbf{I}_{n+1}] \mathbf{A}_s(\boldsymbol{\varphi}) \\ c_d [\mathbf{0}_{1 \times 2n+1} & \mathbf{1}] + k_d [\mathbf{0}_{1 \times n} & \mathbf{1} & \mathbf{0}_{1 \times n+1}] \end{bmatrix} \end{aligned} \quad (\text{A.5})$$

with definition of auxiliary matrix $\mathbf{M}_t(\boldsymbol{\varphi})$ as:

$$\mathbf{M}_t(\boldsymbol{\varphi}) = \begin{bmatrix} \mathbf{M}_s + \mathbf{R}_d m_d \mathbf{R}_d^T + \mathbf{R}_c b \mathbf{R}_c^T & m_d \mathbf{R}_d + b \mathbf{R}_c \\ m_d \mathbf{R}_d^T + b \mathbf{R}_c^T & m_d + b \end{bmatrix} \quad (\text{A.6})$$

The definition of the output matrix $\mathbf{C}_s(\boldsymbol{\varphi})$ in this equation corresponds to output variable vector \mathbf{z} that includes inter-storey drift ratios and absolute accelerations for all floors, and forces $f_b(t)$ and $f_d(t)$, respectively.

Combining Eqs. (A.1) and (A.3) leads to augmented state-space representation

$$\begin{aligned} \dot{\mathbf{x}}(t) &= \mathbf{A}(\boldsymbol{\varphi})\mathbf{x}(t) + \mathbf{E}(\boldsymbol{\varphi})w(t) \\ \mathbf{z}(t) &= \mathbf{C}(\boldsymbol{\varphi})\mathbf{x}(t), \end{aligned} \quad (\text{A.7})$$

where

$$\mathbf{x} = \begin{bmatrix} \mathbf{x}_s \\ \mathbf{x}_q \end{bmatrix} \quad \mathbf{A}(\boldsymbol{\varphi}) = \begin{bmatrix} \mathbf{A}_s(\boldsymbol{\varphi}) & \mathbf{E}_s(\boldsymbol{\varphi})\mathbf{C}_q \\ \mathbf{0}_{n_q \times n_s} & \mathbf{A}_q \end{bmatrix} \quad \mathbf{E} = \begin{bmatrix} \mathbf{0}_{n_s \times 1} \\ \mathbf{E}_q \end{bmatrix} \quad \mathbf{C}(\boldsymbol{\varphi}) = \begin{bmatrix} \mathbf{C}_s(\boldsymbol{\varphi}) & \mathbf{0}_{n_s \times n_q} \end{bmatrix} \quad (\text{A.8})$$

Appendix B. Stationary statistics estimation

This appendix discusses the estimation of the statistical quantities needed to calculate the different performance objectives examined in Section 4.2 for a linear structure under stationary excitation. The augmented state-space description of Eq. (A.7) is leveraged, allowing for an efficient estimation of all quantities through the combination of the structure and excitation representations [42], whereas results are presented for the augmented output vector \mathbf{z} defined in Appendix A. As this vector included both the EDPs and the device control forces, the statistics needed in Section 4.2. for each type of output are obtained by simply examining this specific output instead of the entire augmented vector \mathbf{z} .

Focusing first on the second-order statistics, the output $\mathbf{z}(t)$ of the system of Eq. (A.8) is a zero-mean Gaussian vector with covariance matrix

$$\mathbf{K}_{zz}(\boldsymbol{\varphi}) = \mathbf{C}(\boldsymbol{\varphi})\mathbf{P}(\boldsymbol{\varphi})\mathbf{C}(\boldsymbol{\varphi})^T \quad (\text{B.1})$$

where $\mathbf{P}(\boldsymbol{\varphi})$ is the state covariance matrix, obtained by the solution of the algebraic Lyapunov equation [73]:

$$\mathbf{A}(\boldsymbol{\varphi})\mathbf{P}(\boldsymbol{\varphi}) + \mathbf{P}(\boldsymbol{\varphi})\mathbf{A}(\boldsymbol{\varphi})^T + \mathbf{E}(\boldsymbol{\varphi})\mathbf{E}(\boldsymbol{\varphi})^T = 0 \quad (\text{B.2})$$

The variance $\sigma_{z_i}^2(\boldsymbol{\varphi})$ of the i th output component z_i of vector \mathbf{z} corresponds to the i th element of the diagonal of the covariance matrix \mathbf{K}_{zz} given by Eq. (B.1). These variances are the only quantities needed for the average performance quantification discussed in Section 4.2, accommodating a highly efficient numerical estimation of the objective functions, and solution of the associated optimization problem.

The risk-based quantification requires, additionally estimation of the first-passage probabilities and of the peak response factors. The first-passage probabilities for output z_i over threshold β (in Eq. (15) this is applied for threshold β_i^j with z_i corresponding to edp_i) can be approximated by [87]:

$$P_i(\boldsymbol{\varphi} | \beta, T) = 1 - e^{-v_i^+(\boldsymbol{\varphi}, \beta)T} \quad (\text{B.3})$$

utilizing the conditional out-crossing rate

$$v_i^+(\boldsymbol{\varphi}, \beta) = \lambda_i(\boldsymbol{\varphi}, \beta)r_i^+(\boldsymbol{\varphi}, \beta) \quad (\text{B.4})$$

where, $r_i^+(\boldsymbol{\varphi}, \beta)$ is Rice's unconditional out-crossing rate [88], and $\lambda_i(\boldsymbol{\varphi}, \beta)$ is a temporal-correlation correction factor [73]. The unconditional outcrossing rate is given by

$$r_i^+(\boldsymbol{\varphi}, \beta) = \frac{\sigma_{\dot{z}_i}(\boldsymbol{\varphi})}{\pi\sigma_{z_i}(\boldsymbol{\varphi})} e^{-\frac{\beta^2}{2\sigma_{z_i}^2(\boldsymbol{\varphi})}} \quad (\text{B.5})$$

where $\sigma_{\dot{z}_i}^2$ is the variance of \dot{z}_i , corresponding to the i th diagonal element of the covariance matrix of $\dot{\mathbf{z}}$, given by:

$$\mathbf{K}_{\dot{z}\dot{z}}(\boldsymbol{\varphi}) = \mathbf{C}(\boldsymbol{\varphi})\mathbf{A}(\boldsymbol{\varphi})\mathbf{P}(\boldsymbol{\varphi})\mathbf{A}(\boldsymbol{\varphi})^T \mathbf{C}(\boldsymbol{\varphi})^T \quad (\text{B.6})$$

assuming that the condition $\mathbf{C}(\boldsymbol{\varphi})\mathbf{E}(\boldsymbol{\varphi})=0$ holds [42]. For the temporal correction factor, the one proposed by Taflanidis and Beck [87] is adopted here, given by:

$$\lambda_i(\boldsymbol{\varphi}, \beta) \approx \frac{1 - \exp\left\{-q(\boldsymbol{\varphi})^{0.6} \left(\frac{2}{\sqrt{\pi}}\right)^{0.1} \frac{\beta\sqrt{2}}{\sigma_{z_i}(\boldsymbol{\varphi})}\right\}}{1 - \exp\left\{-\frac{\beta^2}{2\sigma_{z_i}^2(\boldsymbol{\varphi})}\right\}}; \quad q(\boldsymbol{\varphi}) = \frac{\sigma_{z_i}^6(\boldsymbol{\varphi})}{4\pi \int_{-\infty}^{\infty} |\omega| S_{z_i z_i}(\omega | \boldsymbol{\varphi}) d\omega \int_{-\infty}^{\infty} S_{z_i z_i}^2(\omega | \boldsymbol{\varphi}) d\omega} \quad (\text{B.7})$$

where $S_{z_i z_i}(\omega | \boldsymbol{\varphi})$ is the spectral density function for z_i which can be calculated as

$$S_{z_i z_i}(\omega | \boldsymbol{\varphi}) = S_w |H_{z_i}(\omega | \boldsymbol{\varphi})|^2 \quad (\text{B.8})$$

with $H_{z_i}(\omega | \boldsymbol{\varphi})$ corresponding to the frequency response function for z_i . Leveraging the state-space formulation of Eq.(A.7) the latter can be obtained as

$$H_{z_i}(\omega | \boldsymbol{\varphi}) = \mathbf{n}_i^T \mathbf{C}(\boldsymbol{\varphi}) [j\omega \mathbf{I}_{n_x} - \mathbf{A}(\boldsymbol{\varphi})]^{-1} \mathbf{E} \quad (\text{B.9})$$

where \mathbf{n}_i is a n_x dimensional vector of zeros with the i th component being one and for this equation $(j)^2 = -1$. The two one-dimensional integrals in the denominator of $q(\boldsymbol{\varphi})$ in Eq. (B.7) are calculated via standard numerical integration, using Eqs. (B.8) and (B.9) to estimate at each desired frequency ω the spectral density.

The peak factor for output z_i is approximated by [89]:

$$p_{z_i}(\boldsymbol{\varphi}, T) = \sqrt{2 \ln v_e(\boldsymbol{\varphi}) T} + \frac{0.5722}{\sqrt{2 \ln v_e(\boldsymbol{\varphi}) T}} \quad (\text{B.10})$$

where

$$v_e(\boldsymbol{\varphi}) = \left(1.63 q_i(\boldsymbol{\varphi})^{0.225} - 0.38\right) \frac{\sigma_{z_i}(\boldsymbol{\varphi})}{\pi \sigma_{z_i}(\boldsymbol{\varphi})} \quad (\text{B.11})$$

and the bandwidth parameter is defined as:

$$q_i(\boldsymbol{\varphi}) = 1 - \frac{\left(\int_{-\infty}^{\infty} |\omega| S_{z_i z_i}(\omega | \boldsymbol{\varphi}) d\omega\right)^2}{\sigma_{z_i} \sigma_{z_i}} \quad (\text{B.12})$$

Evidently the risk-based quantification entails a higher computational cost, as it requires estimation of the transfer function for each output component and numerical integration for the corresponding bandwidth

Patsialis D, Taflanidis AA, Giaralis A (2023) Exploring the impact of excitation and structural response/performance modeling fidelity in the design of seismic protective devices. *Engineering Structures*, Accepted 13/2/2023.

parameter. Depending on the details of the numerical integration (number of integration points) this should represent a moderate only increase of computational burden.

References

- [1] Constantinou M, Symans M. Seismic response of structures with supplemental damping. *The Structural Design of Tall Buildings*. 1993;2:77-92.
- [2] Symans MD, Charney FA, Whittaker AS, Constantinou MC, Kircher CA, Johnson MW et al. Energy Dissipation Systems for Seismic Applications: Current Practice and Recent Developments. *Journal of Structural Engineering*. 2008;134:3-21.
- [3] Christopoulos C, Filiatrault A. Principles of passive supplemental damping and seismic isolation. Pavia, Italy: IUSS Press; 2006.
- [4] Kaynia AM, Veneziano D, Biggs JM. Seismic effectiveness of tuned mass dampers. *Journal of the Structural Division*. 1981;107:1465-84.
- [5] Matta E, De Stefano A. Seismic performance of pendulum and translational roof-garden TMDs. *MSSP*. 2009;23:908-21.
- [6] Hoang N, Fujino Y, Warnitchai P. Optimal tuned mass damper for seismic applications and practical design formulas. *Engineering Structures*. 2008;30:707-15.
- [7] Soto-Brito R, Ruiz SE. Influence of ground motion intensity on the effectiveness of tuned mass dampers. *Earthquake engineering & structural dynamics*. 1999;28:1255-71.
- [8] Tributsch A, Adam C. Evaluation and analytical approximation of Tuned Mass Damper performance in an earthquake environment. *Smart Structures and Systems*. 2012;10:155-79.
- [9] Marian L, Giaralis A. Optimal design of a novel tuned mass-damper-inerter (TMDI) passive vibration control configuration for stochastically support-excited structural systems. *PrEM*. 2014;38:156-64.
- [10] Ikago K, Saito K, Inoue N. Seismic control of single-degree-of-freedom structure using tuned viscous mass damper. *Earthquake Engineering & Structural Dynamics*. 2012;41:453-74.
- [11] Lazar IF, Neild SA, Wagg DJ. Using an inerter-based device for structural vibration suppression. *Earthquake Engineering & Structural Dynamics*. 2013;43:1129-47.
- [12] Takewaki I. Optimal damper placement for minimum transfer functions. *Earthquake Engineering & Structural Dynamics*. 1997;26:1113-24.
- [13] Sadek F, Mohraz B, Taylor AW, Chung RM. A method of estimating the parameters of tuned mass dampers for seismic applications. *Earthquake Engineering & Structural Dynamics*. 1997;26:617-35.
- [14] Fujino Y, Abé M. Design formulas for tuned mass dampers based on a perturbation technique. *Earthquake engineering & structural dynamics*. 1993;22:833-54.
- [15] Shen W, Niyitangamahoro A, Feng Z, Zhu H. Tuned inerter dampers for civil structures subjected to earthquake ground motions: optimum design and seismic performance. *Engineering Structures*. 2019;198:109470.
- [16] Wang Z, Giaralis A. Enhanced motion control performance of the tuned mass damper inerter through primary structure shaping. *Structural Control and Health Monitoring*. 2021;28:e2756.
- [17] Whittle J, Williams M, Karavasilis TL, Blakeborough A. A comparison of viscous damper placement methods for improving seismic building design. *Journal of Earthquake Engineering*. 2012;16:540-60.
- [18] Ramirez OM, Constantinou MC, Gomez JD, Whittaker AS, Chrysostomou CZ. Evaluation of simplified methods of analysis of yielding structures with damping systems. *Earthquake Spectra*. 2002;18:501-30.
- [19] Marano G, Trentadue F, Greco R. Stochastic optimum design criterion for linear damper devices for seismic protection of buildings. *Structural and Multidisciplinary Optimization*. 2007;33:441-55.

Patsialis D, Taflanidis AA, Giaralis A (2023) Exploring the impact of excitation and structural response/performance modeling fidelity in the design of seismic protective devices. *Engineering Structures*, Accepted 13/2/2023.

- [20] Singh MP, Moreschi LM. Optimal placement of dampers for passive response control. *Earthquake Engineering & Structural Dynamics*. 2002;31:955-76.
- [21] Javidialesaadi A, Wierschem NE. Design and performance evaluation of inerter-based tuned mass dampers for a ground acceleration excited structure. *Soil Dynamics and Earthquake Engineering*. 2021;140:106463.
- [22] Taflanidis AA, Scruggs JT, Beck JL. Reliability-based performance objectives and probabilistic robustness in structural control applications. *Journal of Engineering Mechanics*. 2008;134:291-301.
- [23] Papadimitriou C, Katafygiotis LS, Au SK. Effects of structural uncertainties on TMD design: A reliability based approach. *Journal of Structural Control*. 1997;4:65-88.
- [24] Giaralis A, Taflanidis A. Optimal tuned mass-damper-inerter (TMDI) design for seismically excited MDOF structures with model uncertainties based on reliability criteria. *Structural Control and Health Monitoring*. 2018;25:e2082.
- [25] Radu A, Lazar IF, Neild SA. Performance-based seismic design of tuned inerter dampers. *Structural Control and Health Monitoring*. 2019;26:e2346.
- [26] Taflanidis AA, Giaralis A, Patsialis D. Multi-objective optimal design of inerter-based vibration absorbers for earthquake protection of multi-storey building structures. *Journal of the Franklin Institute*. 2019;356:7754-84.
- [27] Idels O, Lavan O. Optimization-based seismic design of steel moment-resisting frames with nonlinear viscous dampers. *Structural Control and Health Monitoring*. 2021;28:e2655.
- [28] Lin TK, Hwang JS, Chen KH. Optimal distribution of damping coefficients for viscous dampers in buildings. *IJSSD*. 2017;17:1750054.
- [29] Pollini N, Lavan O, Amir O. Optimization-based minimum-cost seismic retrofitting of hysteretic frames with nonlinear fluid viscous dampers. *Earthquake Engineering & Structural Dynamics*. 2018;47:2985-3005.
- [30] Salvi J, Rizzi E. Optimum earthquake-tuned TMDs: seismic performance and new design concept of balance of split effective modal masses. *Soil Dynamics and Earthquake Engineering*. 2017;101:67-80.
- [31] Salvi J, Pioldi F, Rizzi E. Optimum tuned mass dampers under seismic soil-structure interaction. *Soil Dynamics and Earthquake Engineering*. 2018;114:576-97.
- [32] Tubaldi E, Barbato M, Dall'Asta A. Performance-based seismic risk assessment for buildings equipped with linear and nonlinear viscous dampers. *Engineering Structures*. 2014;78:90-9.
- [33] Taflanidis AA, Beck JL. Life-cycle cost optimal design of passive dissipative devices. *Structural Safety*. 2009;31:508-22.
- [34] Gidarlis I, Taflanidis AA, Mavroeidis GP. Multiobjective design of supplemental seismic protective devices utilizing lifecycle performance criteria. *Journal of Structural Engineering*. 2018;144:04017225.
- [35] Ruiz R, Taflanidis A, Giaralis A, Lopez-Garcia D. Risk-informed optimization of the tuned mass-damper-inerter (TMDI) for the seismic protection of multi-storey building structures. *Engineering Structures*. 2018;177:836-50.
- [36] Wong KK. Seismic energy dissipation of inelastic structures with tuned mass dampers. *Journal of Engineering Mechanics*. 2008.
- [37] Lavan O. A methodology for the integrated seismic design of nonlinear buildings with supplemental damping. *Structural Control and Health Monitoring*. 2015;22:484-99.
- [38] Patsialis D, Taflanidis A, Giaralis A. Tuned-mass-damper-inerter optimal design and performance assessment for multi-storey hysteretic buildings under seismic excitation. *Bulletin of Earthquake Engineering*. 2021:1-36.
- [39] Idels O, Lavan O. Performance-based seismic retrofitting of frame structures using negative stiffness devices and fluid viscous dampers via optimization. *Earthquake Engineering & Structural Dynamics*. 2021;50:3116-37.
- [40] Levy R, Lavan O. Quantitative comparison of optimization approaches for the design of supplemental damping in earthquake engineering practice. *Journal of structural engineering*. 2009;135:321-5.

Patsialis D, Taflanidis AA, Giaralis A (2023) Exploring the impact of excitation and structural response/performance modeling fidelity in the design of seismic protective devices. *Engineering Structures*, Accepted 13/2/2023.

- [41] Gidaris I, Taflanidis AA. Performance assessment and optimization of fluid viscous dampers through life-cycle cost criteria and comparison to alternative design approaches. *Bulletin of Earthquake Engineering*. 2015;13:1003-28.
- [42] Taflanidis AA, Scruggs JT. Performance measures and optimal design of linear structural systems under stochastic stationary excitation. *Struct Saf*. 2010;32:305-15.
- [43] Marian L, Giaralis A. Optimal design of inerter devices combined with TMDs for vibration control of buildings exposed to stochastic seismic excitations. 11th International Conference on Structural Safety and Reliability. New York, US2013. p. 1025-32.
- [44] McKenna F. OpenSees: A framework for earthquake engineering simulation. *Computing in Science and Engineering*. 2011;13:58-66.
- [45] Patsialis D, Taflanidis A. Reduced order modeling of hysteretic structural response and applications to seismic risk assessment. *Engineering Structures*. 2020;209:110135.
- [46] Saitua F, Lopez-Garcia D, Taflanidis AA. Optimization of height-wise damper distributions considering practical design issues. *Engineering Structures*. 2018;173:768-86.
- [47] Nagarajaiah S, Narasimhan S, Johnson E. Structural control benchmark problem: Phase II—Nonlinear smart base-isolated building subjected to near-fault earthquakes. *Structural Control and Health Monitoring*. 2008;15:653-6.
- [48] Gonzalez-Buelga A, Lazar IF, Jiang JZ, Neild SA, Inman DJ. Assessing the effect of nonlinearities on the performance of a tuned inerter damper. *Structural Control and Health Monitoring*. 2017;24:e1879.
- [49] Pietrosanti D, De Angelis M, Giaralis A. Experimental study and numerical modeling of nonlinear dynamic response of SDOF system equipped with tuned mass damper inerter (TMDI) tested on shaking table under harmonic excitation. *International Journal of Mechanical Sciences*. 2020;184:105762.
- [50] De Domenico D, Deastra P, Ricciardi G, Sims ND, Wagg DJ. Novel fluid inerter based tuned mass dampers for optimised structural control of base-isolated buildings. *Journal of the Franklin Institute*. 2019;356:7626-49.
- [51] Pietrosanti D, De Angelis M, Giaralis A. Experimental seismic performance assessment and numerical modelling of nonlinear inerter vibration absorber (IVA)-equipped base isolated structures tested on shaking table. *Earthquake Engineering & Structural Dynamics*. 2021.
- [52] Tubaldi E, Kougioumtzoglou IA. Nonstationary stochastic response of structural systems equipped with nonlinear viscous dampers under seismic excitation. *Earthquake Engineering & Structural Dynamics*. 2015;44:121-38.
- [53] Altieri D, Tubaldi E, De Angelis M, Patelli E, Dall'Asta A. Reliability-based optimal design of nonlinear viscous dampers for the seismic protection of structural systems. *Bulletin of Earthquake Engineering*. 2018;16:963-82.
- [54] Clough RW, Penzien J. *Dynamics of structures*. New York, N.Y: McGraw-Hill Inc.; 1993.
- [55] Boore DM. Simulation of ground motion using the stochastic method. *PApGe*. 2003;160:635-76.
- [56] Vetter C, Taflanidis A. Comparison of alternative stochastic ground motion models for seismic risk characterization. *Soil Dynamics and Earthquake Engineering*. 2014;58:48-65.
- [57] Giaralis A, Spanos PD. Derivation of response spectrum compatible non-stationary stochastic processes relying on Monte Carlo-based peak factor estimation. *Earthquakes and Structures*. 2012;3:581-609.
- [58] Lin T, Haselton CB, Baker JW. Conditional spectrum-based ground motion selection. Part I: Hazard consistency for risk-based assessments. *Earthquake Engineering and Structural Dynamics*. 2013;42:1847-65.
- [59] Jalayer F, Beck JL. Effects of two alternative representations of ground-motion uncertainty in probabilistic seismic demand assessment of structures. *Earthquake Engineering and Structural Dynamics*. 2008;37:61-79.
- [60] Housner G, Jennings PC. Generation of artificial earthquakes. *Journal of the Engineering Mechanics Division*. 1964;90:113-52.

Patsialis D, Taflanidis AA, Giaralis A (2023) Exploring the impact of excitation and structural response/performance modeling fidelity in the design of seismic protective devices. *Engineering Structures*, Accepted 13/2/2023.

- [61] Huang Y-N, Whittaker AS, Luco N, Hamburger RO. Scaling earthquake ground motions for performance-based assessment of buildings. *Journal of Structural Engineering*. 2011;137:311-21.
- [62] Whittaker A, Atkinson G, Baker J, Bray J, Grant D, Hamburger R et al. Selecting and scaling earthquake ground motions for performing response-history analyses. Gaithersburg, MD: National Institute of Standards and Technology; 2011.
- [63] Katsanos EI, Sextos AG, Manolis GD. Selection of earthquake ground motion records: A state-of-the-art review from a structural engineering perspective. *Soil Dynamics and Earthquake Engineering*. 2010;30:157-69.
- [64] Kohrangi M, Vamvatsikos D, Bazzurro P. Pulse-like versus non-pulse-like ground motion records: spectral shape comparisons and record selection strategies. *Earthquake Engineering & Structural Dynamics*. 2019;48:46-64.
- [65] FEMA-P-58. Seismic performance assessment of buildings. Redwood City, CA: American Technology Council; 2012.
- [66] Tehrani M, Harvey Jr P, Gavin H, Mirza A. Inelastic condensed dynamic models for estimating seismic demands for buildings. *Engineering Structures*. 2018;177:616-29.
- [67] Pietrosanti D, De Angelis M, Basili M. Optimal design and performance evaluation of systems with Tuned Mass Damper Inerter (TMDI). *Earthquake Engineering & Structural Dynamics*. 2017;46:1367-88.
- [68] Ikago K, Sugimura Y, Saito K, Inoue N. Seismic displacement control of multiple-degree-of-freedom structures using tuned viscous mass dampers. 8th International Conference on Structural Dynamics. Leuven, Belgium.2011. p. 1800-7.
- [69] Smith MC. Synthesis of mechanical networks: the inerter. *Automatic Control, IEEE Transactions on*. 2002;47:1648-62.
- [70] Patsialis D, Kyprioti AP, Taflanidis AA. Bayesian calibration of hysteretic reduced order structural models for earthquake engineering applications. *Engineering Structures*. 2020;224:111204.
- [71] Goulet CA, Haselton CB, Mitrani-Reiser J, Beck JL, Deierlein G, Porter KA et al. Evaluation of the seismic performance of code-conforming reinforced-concrete frame building-From seismic hazard to collapse safety and economic losses. *Earthquake Engineering and Structural Dynamics*. 2007;36:1973-97.
- [72] Porter KA, Kiremidjian AS, LeGrue JS. Assembly-based vulnerability of buildings and its use in performance evaluation. *Earthquake Spectra*. 2001;18:291-312.
- [73] Lutes LD, Sarkan S. Random vibrations : analysis of structural and mechanical systems. Amsterdam ; Boston: Elsevier; 2004.
- [74] Yang JN, Lin S, Kim JH, Agrawal AK. Optimal design of passive energy dissipation systems based on H_{∞} and H_2 performances. *Earthquake Engineering & Structural Dynamics*. 2002;31:921-36.
- [75] Levine W, Athans M. On the determination of the optimal constant output feedback gains for linear multivariable systems. *IEEE Transactions on Automatic Control*. 1970;15:44-8.
- [76] Dorato P, Abdallah C, Cerone V. Linear-quadratic control: An introduction: Prentice Hall; 1998.
- [77] Der Kiureghian A. Structural response to stationary excitation. *Journal of Engineering Mechanics, ASCE*. 1980;106:1195-213.
- [78] Baker JW, Cornell CA. Uncertainty propagation in probabilistic seismic loss estimation. *Structural Safety*. 2008;30:236-52.
- [79] Vamvatsikos D. Derivation of new SAC/FEMA performance evaluation solutions with second-order hazard approximation. *Earthquake Engineering & Structural Dynamics*. 2013;42:1171-88.
- [80] Karnopp DC. Random search techniques for optimization problems. *Automatica*. 1963;1:111-21.
- [81] Beyer K, Bommer JJ. Selection and scaling of real accelerograms for bi-directional loading: a review of current practice and code provisions. *Journal of earthquake engineering*. 2007;11:13-45.

Patsialis D, Taflanidis AA, Giaralis A (2023) Exploring the impact of excitation and structural response/performance modeling fidelity in the design of seismic protective devices. *Engineering Structures*, Accepted 13/2/2023.

[82] Jalayer F, Elefante L, Iervolino I, Manfredi G. Knowledge-based performance assessment of existing RC buildings. *Journal of Earthquake Engineering*. 2011;15:362-89.

[83] Ohtori Y, Christenson R, Spencer Jr B, Dyke S. Benchmark control problems for seismically excited nonlinear buildings. *Journal of Engineering Mechanics*. 2004;130:366-85.

[84] Watson-Lamprey J, Abrahamson N. Selection of ground motion time series and limits on scaling. *Soil Dynamics and Earthquake Engineering*. 2006;26:477-82.

[85] Ruiz R, Taflanidis AA, Lopez-Garcia D, Vetter CR. Life-cycle based design of mass dampers for the Chilean region and its application for the evaluation of the effectiveness of tuned liquid dampers with floating roof. *Bulletin of Earthquake Engineering*. 2016;14:943-70.

[86] Lin CC, Chen CL, Wang JF. Vibration control of structures with initially accelerated passive tuned mass dampers under near-fault earthquake excitation. *Computer-Aided Civil and Infrastructure Engineering*. 2010;25:69-75.

[87] Taflanidis AA, Beck JL. Analytical approximation for stationary reliability of certain and uncertain linear dynamic systems with higher dimensional output. *Earthquake Engineering and Structural Dynamics*. 2006;35:1247-67.

[88] Rice SO. Mathematical analysis of random noise. *Bell System Technical Journal*. 1944, 1945;23 and 24.

[89] Kiureghian AD. A response spectrum method for random vibration analysis of MDF systems. *Earthquake Engineering & Structural Dynamics*. 1981;9:419-35.